

Available online at www.sciencedirect.com**ScienceDirect**Journal homepage: www.elsevier.com/locate/cortex**Clinical neuroanatomy****Cytoarchitecture and probability maps of the human medial orbitofrontal cortex**

Anton Henssen ^{a,1}, Karl Zilles ^{b,c,d,*1}, Nicola Palomero-Gallagher ^b,
Axel Schleicher ^b, Hartmut Mohlberg ^b, Fatma Gerboga ^a,
Simon B. Eickhoff ^{b,e}, Sebastian Bludau ^b and Katrin Amunts ^{a,b}

^a C. and O. Vogt Institute for Brain Research, Heinrich Heine University Düsseldorf, Germany

^b Institute for Neuroscience and Medicine (INM-1), Research Centre Jülich, Jülich, Germany

^c Department of Psychiatry, Psychotherapy and Psychosomatics, University Hospital Aachen, RWTH Aachen University, Germany

^d JARA Brain, Research Centre Jülich, Jülich, Germany

^e Institute of Clinical Neuroscience and Medical Psychology, Heinrich-Heine University, Düsseldorf, Germany

ARTICLE INFO**Article history:**

Received 20 April 2015

Reviewed 16 July 2015

Revised 11 September 2015

Accepted 9 November 2015

Action editor Marco Catani

Published online 2 December 2015

ABSTRACT

Previous architectonical studies of human orbitofrontal cortex (OFC) provided divergent maps regarding number, location, and extent of areas. To solve this controversy, an observer-independent cytoarchitectonical mapping of medial OFC (mOFC) was performed. Borders of cortical areas were detected in histological sections of ten human post-mortem brains using a quantitative, statistically testable method, and their stereotaxic localization and intersubject variability were determined.

Three areas were identified: granular Fo1 mainly on the rostral Gyrus rectus and medial of the olfactory sulcus; granular to dysgranular Fo2, mainly on the posterior part of the ventromedial Gyrus rectus and the medial and lateral banks of the olfactory sulcus; granular Fo3 between the olfactory and medial or intermediate orbital sulci. Fo3 was bordered medially by Fo1 and Fo2 and laterally by the lateral OFC (lOFC).

A cluster analysis of the cytoarchitectonical features of Fo1-Fo3, subgenual cingulate areas, BA12, lateral and medial areas of the frontopolar cortex, lOFC and areas of Broca's region demonstrated the cytoarchitectonical similarity between the mOFC areas in contrast to all other frontal areas.

Probabilistic maps of mOFC areas show a considerable intersubject variability in extent and position in stereotaxic space, and provide spatial templates for anatomical localization of *in vivo* neuroimaging data via the JuBrain atlas and the Anatomy Toolbox.

© 2015 Elsevier Ltd. All rights reserved.

* Corresponding author. Institute for Neuroscience and Medicine (INM-1), Research Centre Jülich, D-52425 Jülich, Germany.

E-mail address: k.zilles@fz-juelich.de (K. Zilles).

¹ These authors contributed equally to this work.

<http://dx.doi.org/10.1016/j.cortex.2015.11.006>

0010-9452/© 2015 Elsevier Ltd. All rights reserved.

1. Introduction

The orbitofrontal cortex (OFC) is involved in a variety of functions associated with pleasant as well as painful perceptions and reward processing (Aharon et al., 2001; Blood, Zatorre, Bermudez, & Evans, 1999; Frey & Petrides, 2000; Grabenhorst & Rolls, 2009; Grabenhorst, Rolls, & Bilderbeck, 2008; Grabenhorst, Rolls, Margot, da Silva, & Velazco, 2007; Grabenhorst, Rolls, Parris, & d'Souza, 2010; O'Doherty, Kringelbach, Rolls, Hornak, & Andrews, 2001; O'Doherty, Winston, et al., 2003; O'Doherty, Dayan, Friston, Critchley, & Dolan, 2003; Rolls, 2000, 2004b, 2007; Rolls & Baylis, 1994; Rolls, Kringelbach & de Araujo et al., 2003; Rolls, O'Doherty, et al., 2003). Olfactory and gustatory stimuli elicit activations in the OFC (de Araujo, Kringelbach, Rolls, & Hobden, 2003; de Araujo, Kringelbach, Rolls, & McGlone, 2003; de Araujo, Rolls, Kringelbach, McGlone, & Phillips, 2003; Gottfried, Deichmann, Winston, & Dolan, 2002; Gottfried, O'Doherty, & Dolan, 2002; Kringelbach, O'Doherty, Rolls, & Andrews, 2003; Rolls, 2004a; Small, Jones-Gotman, Zatorre, Petrides, & Evans, 1997; Small et al., 1999), which are often associated with hedonistic aspects. The OFC is also involved in touch and pain processing (Lorenz, Minoshima, & Casey, 2003; Rolls, Kringelbach, et al., 2003; Rolls, O'Doherty, et al., 2003).

Anatomical and functional studies have shown that the OFC must be subdivided at least into a medial (mOFC) and a lateral part (lOFC). Although the OFC's sulcal pattern is variable across subjects (Chi, Dooling, & Gilles, 1977; Chiavaras, LeGoualher, Evans, & Petrides, 2001; Chiavaras & Petrides, 2000; Eberstaller, 1890), the olfactory, medial orbital, intermediate orbital, transverse and lateral orbital sulci are frequently identifiable. The OFC can be macroscopically subdivided by its sulcal pattern into a medial part (mOFC) located between the medial orbital and the inferior rostral sulci (Sanides, 1962), and a lateral part (lOFC) located between the medial or intermediate and lateral orbital sulci. However, the expression and patterns of the medial and intermediate orbital sulci are highly variable (Chiavaras & Petrides, 2000), and therefore do not provide a consistent and easily identifiable landmark for the identification of the border between mOFC and lOFC.

The most convincing arguments for a subdivision of OFC can be derived from architectonic and functional studies. According to Brodmann's map (Brodmann, 1909), three cytoarchitectonical areas occupy the total ventral surface of the frontal lobe: a part of BA10 ("Area frontopolaris"), the complete BA11 ("Area praefrontalis"), and the medial part of BA47 ("Area orbitalis"; Fig. 1A). The borders of BA11 are approximately defined by the superior rostral sulcus medially (Brodmann, 1910), the fronto-marginal sulcus rostrally, and the medial orbital sulcus on the orbital surface. The homotypical (six-layered) isocortical area BA11 completely covers mOFC, whereas BA47 occupies lOFC and extends onto the orbital part of the inferior frontal gyrus. BA11 and BA47 were described by Brodmann (1909) as cytoarchitectonically distinct areas, which are well delineable. BA11 is identical with the cyto- and myeloarchitectonically defined orbitomedian zone OmZ (Fig. 1J; red circled area) of Sanides (1962). The posterior part of mOFC extends to the

olfactory and insular cortex and is partly covered by the temporal lobe. The parolfactory sulcus often marks the border between mOFC and BA25 (Brodmann, 1909, 1910). BA10 clearly exceeds the orbital surface, and constitutes the frontopolar region, which is characterized by a conspicuous layer IV (Sanides, 1962). Thus, BA10 is not part of the mOFC, where layer IV is by far thinner and less well developed. The caudally adjoining area BA25 is not part of the mOFC either, because this area completely lacks an inner granular layer (layer IV), and thus, differs principally from the six-layered isocortical area BA11.

The existing maps of the human OFC differ, however, with respect to the number of areas identified, their relative size, extent and spatial relationship to each other and to macroscopical landmarks. In contrast to Brodmann's (1909) mosaic of the three areas BA10, BA11, and BA47 on the orbital surface, other authors suggested more areas, subareas and transitional areas (Beck, 1949; von Economo & Koskinas, 1925; Hof, Mufson, & Morrison, 1995; Mackey & Petrides, 2009; Ngowyang, 1934; Öngür, Ferry, & Price, 2003; Petrides & Pandya, 1994; Sanides, 1962; Sarkisov, Filimonoff, & Preobrashenskaya, 1949; Strasburger, 1937; Uylings et al., 2010; Vogt, 1910; Vogt & Vogt, 1919, Fig. 1). In these cases, additional letters and numerals indicated cytoarchitectonical similarities or distinctions. Since the intersubject variability of cytoarchitecture was not considered in any of these maps, it is difficult to decide whether at least some of the subareas or transition zones are only a result of local variations within a cytoarchitectonical entity. Therefore, aim of the present study was to analyze the cytoarchitecture of the medial part of the OFC by a quantitative observer-independent and statistically testable method for identification of areal borders and definition of intersubject variability.

The structural segregation of OFC by architectonic analysis is further supported by connectivity studies, which have mainly been carried out in non-human primates. Monkey mOFC has reciprocal connections with various limbic structures such as anterior cingulate and medial temporal cortices, insula, amygdala, entorhinal cortex, hippocampus, diagonal band of Broca, midline thalamic nuclei and the magnocellular sector of the mediodorsal thalamic nucleus (Barbas, 1992, 2000; Barbas & De Olmos, 1990; Carmichael, Clugnet, & Price, 1994; Carmichael & Price, 1995; Cavada, Company, Tejedor, Cruz-Rizzolo, & Reinoso-Suarez, 2000; Mesulam & Mufson, 1982; Mesulam, Mufson, Levey, & Wainer, 1983; Morecraft, Geula, & Mesulam, 1992; Neubert, Mars, Sallet, & Rushworth, 2015; Öngür & Price, 2000; Pandya, Van Hoesen, & Mesulam, 1981; Seltzer & Pandya, 1989; Vogt & Pandya, 1987; Yeterian & Pandya, 1988). Baylis and colleagues (1995) showed that in primates the OFC receives and integrates inputs from sensory modalities such as taste and olfaction. In addition, auditory (Frey, Kostopoulos, & Petrides, 2000; Janata et al., 2002), visual (Barbas, 1993; Barbas & Pandya, 1987; Carmichael & Price, 1995; Morecraft et al., 1992) and somatosensory (Carmichael & Price, 1995) inputs reach the OFC.

Since all previous maps are only available as two-dimensional schematic drawings, the relation between functional imaging data and cytoarchitectonical maps cannot be directly examined in the same reference space. To overcome these problems, and to create a map applicable to

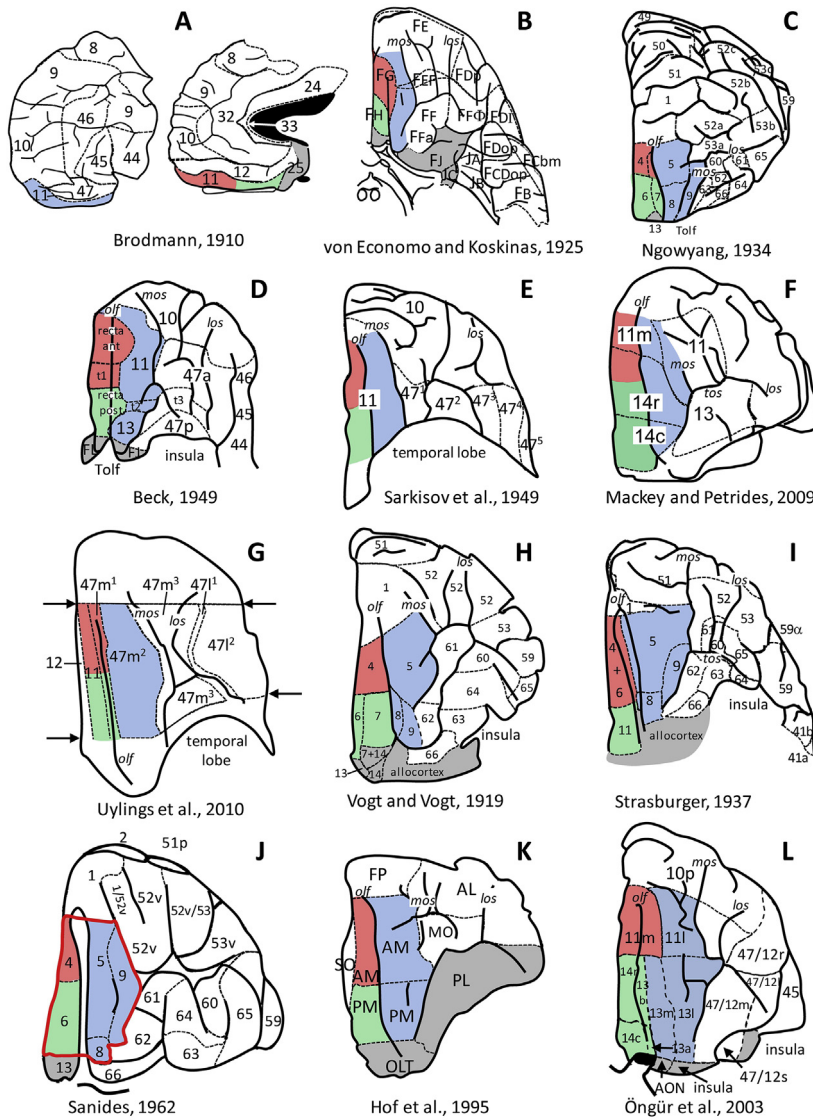


Fig. 1 – Published maps of the orbitofrontal cortex with the putative homologs with the areas Fo1, Fo2 and Fo3 of the present study. A Brodmann (1910; lateral and medial views), B von Economo and Koskinas (1925), C Ngowyang (1934), D Beck (1949), E Sarkisov et al. (1949), F Mackey and Petrides (2009), G Uylings et al. (2010), H Vogt and Vogt (1919), I Strasburger (1937), J Sanides (1962), K Hof et al. (1995), L Öngür et al. (2003). The maps in A–G are based exclusively on cytoarchitectonical studies, the maps in H–I on myeloarchitectonical or combined myelo- and cytoarch studies, and the maps in J–L on combined cytoarchitectonical and immunohistochemical studies. The Arabic numbers in A, D–E, and G, indicate the nomenclature of Brodmann or a nomenclature derived from that, the letter combinations in B are the nomenclature of von Economo and Koskinas (1925), Arabic numbers in C and J–L represent the nomenclature of Vogt and Vogt (1919), and those in F and G are based on Walter's (1940) nomenclature. Cytoarchitectonical analysis in G was restricted to the region located between the arrows. The colors indicate possible homologies with our area Fo1 (red), Fo2 (green), and Fo3 (blue). Gray indicates transition region between iso- and allocortex. AON anterior olfactory nucleus, los lateral orbital sulcus, mos medial orbital sulcus, olf olfactory sulcus, Tolf olfactory tubercle.

functional *in vivo* data, we analyzed the region posterior to the frontopolar BA10, medial to BA47, and rostral to the cingulate cortex in a sample of ten, serially sectioned and cell body-stained post-mortem brains. Then the individual maps were 3D reconstructed and registered to the widely used reference space of the Montreal Neurological Institute (single subject MNI brain; Evans, Janke, Collins, & Baillet, 2012;

Evans et al., 1992) in which probabilistic maps were generated. These maps provide information about intersubject variability in anatomical MNI space (Amunts et al., 2005), and enable a comparison with functional imaging data for subsequent analysis of structure-function relationships (Eickhoff, Heim, Zilles, & Amunts, 2006; Eickhoff et al., 2005, 2007).

2. Material and Methods

2.1. Processing of post-mortem brains

Ten adult brains (5 male, 5 female) were obtained from the body donor program of the University of Düsseldorf in accordance with legal requirements (Table 1). Post-mortem delay was less than 24 h. The clinical records did not show any history of psychiatric or neurological diseases. Brains were fixed in 4% buffered formalin or Bodian's fixative for at least 6 months. To avoid distortions during fixation, brains were suspended by the basilar or vertebral arteries in the fixation fluid.

Histological processing and 3D-reconstruction of the post-mortem brains has been described in detail elsewhere (Amunts et al., 1999; Zilles, Schleicher, Palomero-Gallagher, & Amunts, 2002). In short, MR imaging of the fixed brains was performed on a Siemens 1.5T scanner (Erlangen, Germany) using a T1-weighted 3D FLASH sequence (flip angle 40°, repetition time TR 40 msec, echo time TE 5 msec) before histological processing; these images (MR-image data set) were later used as an undistorted spatial reference for the 3D-reconstruction of the histological sections. The brains were embedded in paraffin, and sectioned in the coronal plane (thickness: 20 µm) using a large-scale microtome. Blockface images of the paraffin embedded brains were acquired at equidistant intervals of 300 µm (blockface data set) during the cutting process. Sections were mounted, stained for cell bodies using a silver staining method (Merker, 1983). Stained sections with an inter-section distance of 1.2 mm were digitized using a flatbed scanner with a resolution of 1,200 dpi. This step provided a digitized data set of the histological sections with an in-plane resolution of 20 µm. The blockface data set was used together with the MR-image data set and the digitized histological sections for the subsequent 3D-reconstruction of the brains.

2.2. Quantification of cytoarchitectonical features

Regions of interest (ROIs) were defined by microscopical inspection of the histological sections. The ROIs were digitized using a CCD camera and a computer-controlled microscope equipped with a scanning stage. The digitized sections were then converted into gray level index (GLI) images (Schleicher

et al., 2000). The GLI is a measure of the volume fraction of cell bodies (Schleicher & Zilles, 1990; Wree, Schleicher, & Zilles, 1982) and was computed in immediately adjacent rectangular fields of 17 µm × 17 µm. The outer (border between layers I and II), and inner (border between layer VI and white matter) contour lines of the cortex were interactively traced in the GLI-images. Based on the Laplace equation, curvilinear traverses, running perpendicular to the cortical layers from the outer to the inner contour (Fig. 2) were calculated (Schleicher et al., 2005). Along these traverses, profiles describing the layer-specific changes in the volume fraction of cell bodies (GLI) were extracted (Fig. 3).

The profiles reflect the volume density of cell bodies throughout the cortical thickness (Schleicher et al., 2005). A feature vector based on the central moments of the original profile was then calculated using the following features of the profile curves: mean GLI, cortical depth of centre of gravity, standard deviation, skewness, and kurtosis, and the respective parameters of the first derivative of the profile (Amunts, Malikovic, Mohlberg, Schormann, & Zilles, 2000; Dixon, 1988; Zilles et al., 2002). The Mahalanobis distance (Mahalanobis, Majumda, & Rao, 1949) served as a multivariate distance measure to quantify differences between adjacent profiles (Schleicher et al., 2000; Schleicher, Amunts, Geyer, Kowalski, & Zilles, 1998; Schleicher, Amunts, Geyer, Morosan, & Zilles, 1999; Schleicher et al., 2005). Areal borders were identified at those positions along the cortical ribbon, where the Mahalanobis distance reached a significant maximum (Fig. 2). The significance was tested with Hotelling's T2-test (Bonferroni correction for multiple comparisons). To make this process more robust against noise in single profiles, adjacent blocks of profiles (each consisting of 5–30 individual profiles) were defined for the calculation of Mahalanobis distances.

A cytoarchitectonical border was accepted at a particular position, if and only if the significant Mahalanobis distance maximum of each of the different block sizes was found at a comparable position in neighboring sections (Schleicher et al., 2005, Figs. 4 and 5). Fig. 5 exemplarily illustrates in five brains the spatial consistency of the observer-independently defined cortical borders of all three mOFC areas in serial histological sections. The spatial relation of the outer border of area Fo3 to the medial orbital sulcus is also illustrated. This approach resulted in an observer-independent delineation of cytoarchitectonically defined areas based on quantitative criteria.

Table 1 – Brains used for cytoarchitectonical analysis of orbitofrontal areas Fo1, Fo2 and Fo3. Case numbering according to designations of the brain bank.

Brain ID	Age (years)	Sex	Brain weight (g)	Cause of death
1	79	f	1350	Carcinoma of the bladder
3	69	m	1360	Cardiovascular disease
4	75	m	1349	Acute glomerulonephritis
5	59	f	1142	Cardiorespiratory insufficiency
6	54	m	1622	Myocardial infarction
8	72	f	1216	Renal failure
9	79	f	1110	Cardiorespiratory insufficiency
11	74	m	1381	Myocardial infarction
13	39	m	1234	Drowning
14	86	f	1113	Cardiorespiratory insufficiency

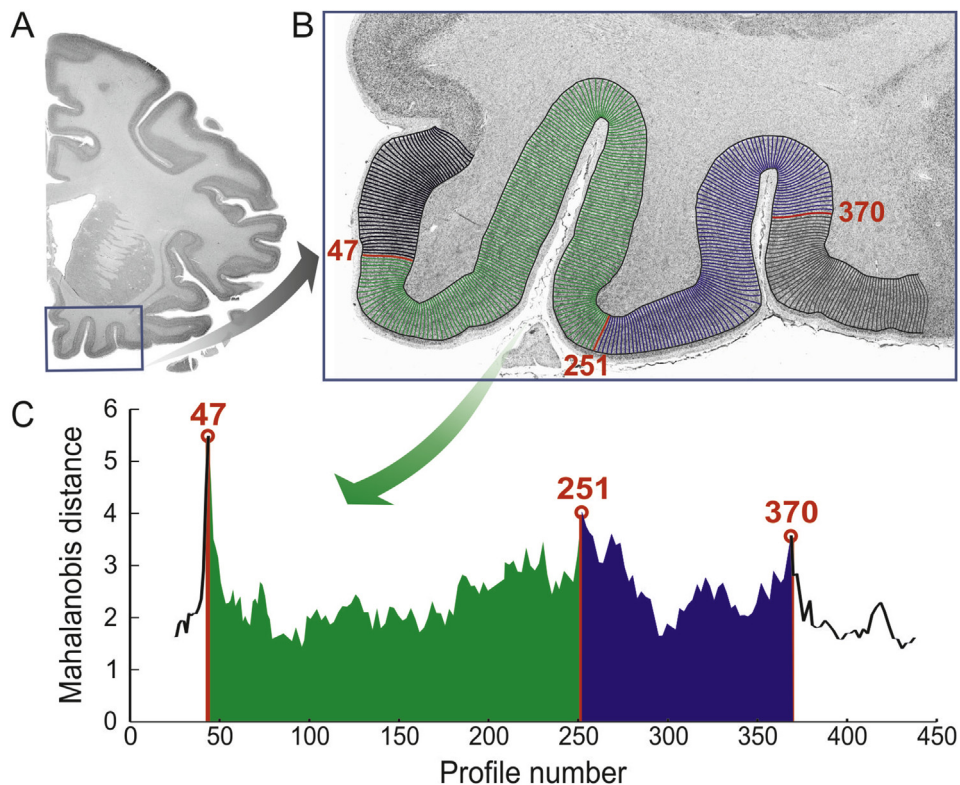


Fig. 2 – Image acquisition and definition of cortical borders in a cell-body stained histological section through the frontal lobe (A). The box marks the region of interest (ROI) for the quantitative, cytoarchitectonical analysis shown in (B–C). B: GLI profiles cover the cortical ROI from the layer I/II border to the cortex/white matter border. The profiles quantify the laminar changes of the GLI from the surface to the white matter (A. Schleicher et al., 1999). Borders between cortical areas were defined at those positions, where the shape of the GLI-profiles changes significantly. These changes are revealed by significant maxima of the Mahalanobis distance. Significant maxima are found at profile positions 47, 251 and 370 (C). Green highlights the extent of Fo1 and blue that of Fo3.

In order to avoid suggestions of unproven homology between the present and previously published cytoarchitectonical maps, a neutral, topographically oriented nomenclature was used for labelling the areas. “F” indicates the location in the frontal lobe, “o” stands for the orbital region, and the numerals define different orbitofrontal areas.

2.3. Probabilistic cytoarchitectonical maps in stereotaxic space

The extent of the delineated areas was manually traced in both hemispheres in the digitized histological sections (Fig. 5), and 3D-reconstructed. Since the cortical areas were traced in digitized images of histological sections at a resolution of 20 μm , these images were down-sampled to enable a registration to the MR volume, which has a resolution of $1 \times 1 \times 1\text{mm}$, thus inevitably introducing continuous values. Application of a nearest neighbor interpolation to continuous values results in a non-continuous distribution of gray values, which would considerably bias subsequent analyses. In this case, nearest-neighbor interpolation introduces a gross overestimation of the size of the area of interest comparable to a partial volume effect. Therefore, we used a trilinear interpolation, which is better suited for the processing of continuous

values because it preserves the smoothness of the values. It is clear, that this method can also lead to an overestimation of the size of the region of interest, but our experience with both approaches in the past has clearly shown that the effect of the trilinear interpolation is much smaller than that of the nearest neighbor interpolation.

The individual cortical areas of the OFC were spatially normalized to the T1-weighted single-subject MNI template brain (Evans et al., 1992, 2012). The spatial shift introduced by the MNI template with respect to the anterior commissure (AC) as the origin of the coordinate system was corrected, and data were normalized to the anatomical MNI space (Amunts et al., 2005). The origin of the original MNI reference space is located 4 mm more caudally (y-axis) and 5 mm more dorsally (z-axis) than that of the anatomical MNI space. The areas of the different brains were superimposed and continuous probabilistic maps were generated in anatomical MNI space. The probabilistic map of a given area shows for each voxel of the reference brain the probability of how many individual post-mortem brains are represented in a particular voxel of the reference brain. Thus, these maps quantitatively express the intersubject variability of a cortical area in stereotaxic space and are available through the JuBrain atlas (<http://www.jubrain.fz-juelich.de/apps/cytoviewer/cytoviewer-main.php>)

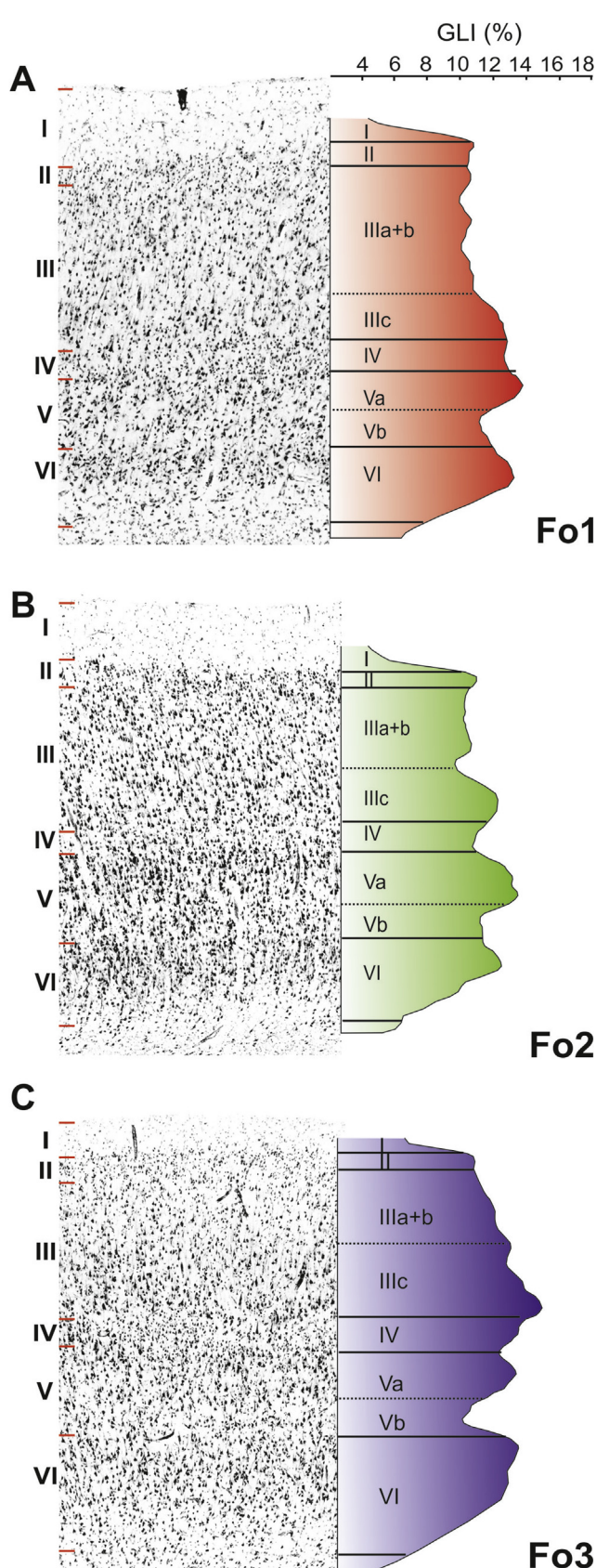
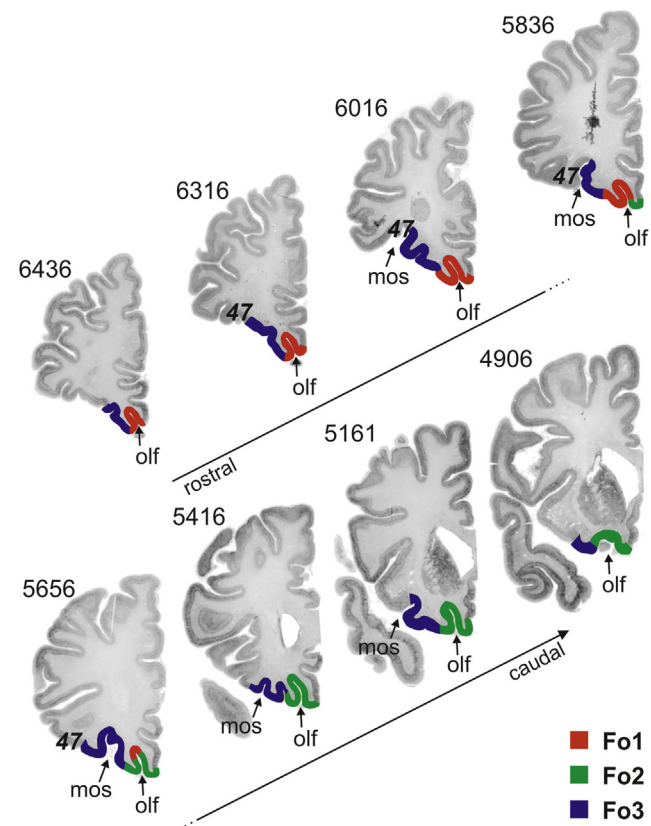


Fig. 3 – Cytoarchitecture of Fo1, Fo2, and Fo3 with corresponding GLI-profiles. Roman numerals indicate cortical layers.



as surface representations. The “maximum probability maps” (MPM) assign to each voxel of the reference space that area, which has the highest probability in that position (Eickhoff et al., 2005, 2006, 2007). If two areas show the same probability at a given voxel, then the voxel is assigned to the region showing the higher average probability in the surrounding 26 voxels (Eickhoff et al., 2005).

Interhemispheric differences in stereotaxic location of identified cytoarchitectonical areas with respect to the anterior–posterior, medial–lateral, and inferior–superior axes were tested by using a repeated measurement two-way analysis of variance (ANOVA) with “area” and “hemisphere” as factors, and “brain” as repeated measurement-factor (Systat® 13 for Windows).

2.4. Volumetry

The volume of a cortical area (V , in mm^3) was calculated based on areal measurements on images of the digitized histological sections:

$$V = s \cdot \Delta x \cdot \Delta y \cdot F \cdot \sum N_i$$

where spacing (s) between two measured sections was 1.2 mm ; pixel size (Δx and Δy) was $.02116 \times .02116 \text{ mm}$; F was

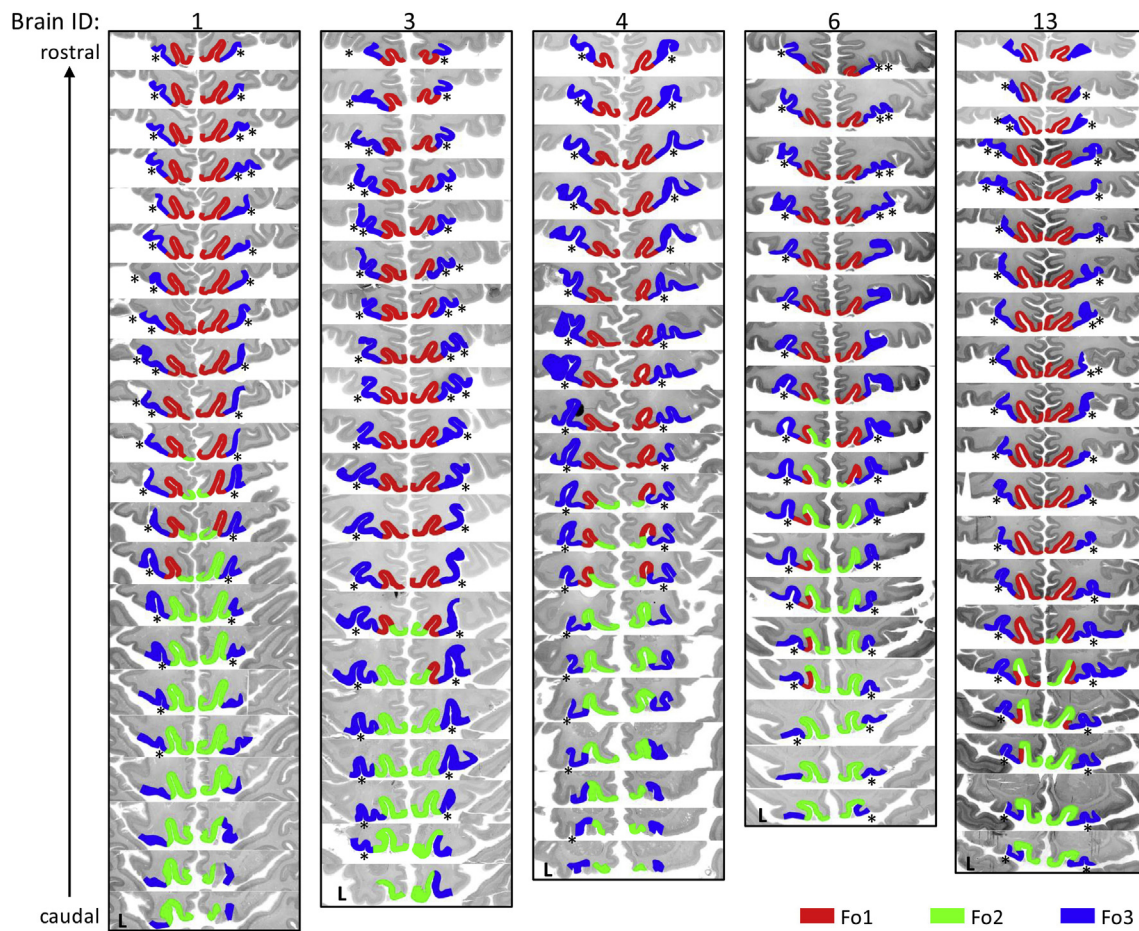


Fig. 5 – Anterior-posterior sequences of coronal histological sections through five exemplary brains (brains 1, 3, 4, 6, 13, see Table 1). Fo1 red, Fo2 green, Fo3 blue. Asterisks mark the medial orbital sulcus. L left hemisphere.

the individual shrinkage factor of each brain caused by the histological processing, and N_i the number of pixels of the cortical area in section i . F was calculated for each individual brain as the ratio between the fresh volume of the brain and its volume after histological processing (Amunts et al., 2005).

Prior to statistical analysis areal volumes were normalized by the individual fresh brain volumes in order to compensate the trend of male brains to larger volumes compared to female brains (Luders, Toga, & Thompson, 2014; Perlaki et al., 2014). The volumes of areas Fo1–Fo3 were then analyzed with respect to sex and interhemispheric (side) differences using Monte-Carlo permutation tests. The difference in the mean volumes between the 5 male and 5 female brains was calculated. Under the null-hypothesis of gender exchangeability, we then randomly reassigned each brain to one of the two groups (male/female), and re-computed the respective difference between the mean volumes of the ensuing randomly assembled groups. This difference obtained under the null-hypothesis (that brain assignment to a gender group is irrelevant) was recorded, and the procedure repeated 106 times. The true gender difference was considered significant if it was larger than 95% of the values under the empirical null-distribution ($p < .05$; Bonferroni corrected for multiple comparisons).

In the analysis of interhemispheric differences a within-subject design was used. We calculated the differences between left and right volumes in each brain. The mean of these differences represents the average interhemispheric difference in the paired-test design. Under the null-hypothesis that there is no difference between the hemispheres and that side-labels may be freely exchangeable, we randomly and independently across subjects designated the two measurements as “left” or “right”. The mean differences between “left” and “right” volumes across subjects were calculated. This is the difference value for each area under the null-hypothesis. This procedure was repeated 106 times and interhemispheric differences were considered significant, if they were larger than 95% of the values under the empirical null-distribution ($p < .05$; Bonferroni corrected for multiple comparisons).

2.5. Hierarchical cluster analysis of cytoarchitectonical similarities between cortical areas

We used a hierarchical cluster analysis for an explorative description of the similarities or dissimilarities in cytoarchitecture between the mOFC areas and numerous neighboring areas. The putative clustering of cortical areas is based on their cytoarchitectonic feature vectors, which were extracted

from the GLI-profiles. The hierarchical clustering agglomerates the cortical areas in a sequence of similarity. Crucial settings in this explorative analysis are the linkage (we used the Ward approach) and the distance (we used the Euclidean distance) to quantify the degree of dissimilarity between cortical areas. Alternative distance measures such as the Minkowski or the City block metrics were also considered, but the Euclidean distance proved to be superior in terms of plausibility of the resulting dendrogram and the cophenetic correlation coefficient used to validate alternative cluster solutions.

Following neighboring areas were included: BA47 laterally adjacent to Fo3; frontopolar areas Fp1 and Fp2 (roughly corresponding to lateral and medial parts of BA10, respectively; Bludau et al., 2014) rostrally adjacent to Fo1 and Fo3; areas s32, s24 and BA25 (Palomero-Gallagher, Mohlberg, Zilles, & Vogt, 2008; Palomero-Gallagher, Vogt, Schleicher, Mayberg, & Zilles, 2009) of the anterior cingulate cortex; BA12; areas BA44 and BA45 of Broca's region (Amunts et al., 1999; Amunts, Schleicher, & Zilles, 2004). In summary, representative blocks of 15–30 GLI-profiles each were extracted from three randomly selected sections of each area and hemisphere of each of the ten brains resulting in 45–90 profiles per area and hemisphere. To reduce data variability, ROIs were collected at sites where the cortex appeared to be sectioned vertical to the surface without any recognizable disturbance of the cytoarchitectonic structure. Including all profiles generated by the parcellation process would decrease the precision of the hemispheric areal feature vector estimate due to the increased variability in the profiles sample. Systat® 13 for Windows was applied for statistical testing and visualization.

3. Results

3.1. Cytoarchitecture of the mOFC and mapping of three areas

Three areas, Fo1, Fo2 and Fo3, were identified on the mOFC (Figs. 3–5). They share some common cytoarchitectonical features, which enable their delineation from neighboring areas. In contrast to the caudally adjacent agranular insular cortex and the allocortical olfactory cortex, areas Fo1–Fo3 have a homotypical cytoarchitecture. I.e., they have a six-layered cortex with an inner granular layer, lamina IV, which is characteristic of the isocortex. The density of granular cells and the width of layer IV, however, differ between the three areas, with Fo2 having the smallest layer IV (Figs. 3 and 6). Additionally, regional variations in cell packing density in layers III and V provide criteria for the distinction between the mOFC areas and area Fo4 (medial part of BA47) of the lOFC as well as the frontopolar isocortex. Typically, layer V of Fo1–Fo3 can be subdivided into layers Va and Vb. Layer Vb is clearly visible as a less cell dense layer between layer Va and upper layer VI, which both show a higher cell packing density (Fig. 3).

3.1.1. Fo1

This area has a less dense but broader layer III than the other mOFC areas (Figs. 3 and 6). The difference in cell density is

particularly obvious by a comparison with Fo2 (Fig. 3). Layer III can be clearly delineated from the thin, but cell dense layer II (Fig. 7). A separation between layers IIIa and IIIb is not clearly detectable in any of the mOFC areas. In Fo1, most of the pyramidal neurons in layer IIIc are larger than those in layer IIIa + b. Granular layer IV in Fo1 is narrower (Fig. 7) and less densely packed than in the rostrally neighboring frontopolar cortex. The pyramidal cells in layer IIIc of Fo1 are of equal size or larger than those of layer Va (Fig. 6). As in all mOFC areas, larger and more densely packed pyramidal cells are found in layer Va than in layer Vb. The cell packing density of layer Va is lower in Fo1 than in Fo2 (Figs. 3 and 6). The difference in cell packing density between Vb and the adjacent layers Va and VI is less pronounced in BA10 compared to area Fo1 (Fig. 7).

Area Fo1 is found on the Gyrus rectus and in the olfactory sulcus (Fig. 4). It extends from the posterior border of areas Fp1 and Fp2 to approximately the level of the Genu corporis callosi and the transverse orbital sulcus. On the mesial hemispheric surface, the rostral part of Fo1 has a border with Fp1, Fp2, and BA12. Its posterior part adjoins cingulate area s32 (Fig. 8). The most posterior portion of the highly variable inferior rostral sulcus indicates the border between the cingulate cortex and Fo1 in the left hemisphere of the reference brain (Fig. 8).

3.1.2. Fo2

In contrast to Fo1 and Fo3, layer IIIc of Fo2 is clearly separated from the adjacent layer IIIa + b by a local minimum of the GLI profile (Fig. 3). The width of layer IV is smaller in Fo2 than in Fo1 (Fig. 6). The density of granular cells in layer IV of Fo2 increases slightly from posterior to anterior and is lower than in Fo1. Even in its most rostral parts, layer IV of Fo2 remains less cell-dense than that of Fo1. The narrowness of layer IV in the most posterior part of Fo2 makes its appearance almost dysgranular, whereas the most anterior part is granular. Fo2 can be delineated from Fo1 and Fo3 by the higher cell density in its layer Va (Figs. 3, 6 and 9). The pyramidal cells in Va of Fo2 are slightly larger than those in IIIc. This relation further distinguishes Fo2 from Fo3, where the pyramids of layer IIIc and Va are of approximately equal size (Fig. 6).

Fo2 medially abuts the cingulate area s32 (Fig. 8). This area shows a higher cell density and wider layer II than Fo2 (Fig. 10). In contrast to the granular layer IV of the posterior part of Fo2, area s32 is dysgranular. In area s32, pyramidal cells from deep layer III and upper layer V invade its layer IV.

Area Fo2 follows Fo1 in caudal direction, and posteriorly reaches the level of the olfactory cortex (Fig. 8). Fo2 occupies the posterior part of the Gyrus rectus, and the medial and lateral banks of the olfactory sulcus. Both Fo1 and Fo2 are followed laterally by area Fo3, which covers major parts of the medial orbitofrontal gyrus and reaches the medial orbital sulcus (Fig. 8). The relation between the lateral cytoarchitectonical border of Fo2 and the medial orbital sulcus varies, however, considerably between the individual brains.

3.1.3. Fo3

Fo3 has large pyramidal cells in layer IIIc, which are more densely packed than those in the medially adjacent areas Fo1 and Fo2 (Figs. 3 and 11). In contrast to the moderately cell dense layer IV of Fo2, the inner granular layer of Fo3 has a higher cell density, and is more prominent in its anterior than

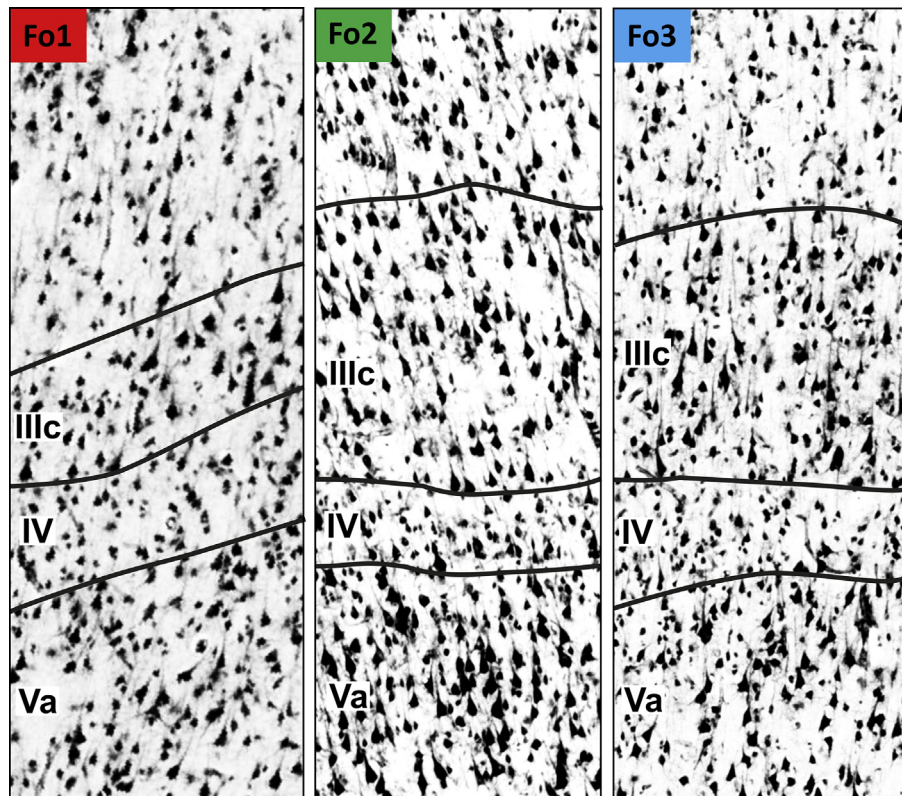


Fig. 6 – Detailed view of layers III–V in areas Fo1, Fo2, and Fo3.

posterior part. The caudally adjoining anterior insular cortex is agranular, and can thus be separated from Fo3, which differs from the laterally adjoining area Fo4 of the lOFC (Fig. 8) with respect to several aspects. One of which is the packing density of large pyramidal cells in layer IIIc, that is lower in Fo3 compared to Fo4. Contrary to that, layer Va of Fo3 shows a higher cell density than the respective layer of Fo4 (Fig. 12). Furthermore, layers II and IV are wider in Fo4 than in Fo3 (Fig. 12). Layer V of Fo4 is not further subdivided due to the overall low cell packing density and small cell sizes across this layer, and thus is less distinct than in Fo3. Fo3 is rostrally bordered by the frontopolar cortex (Fig. 8).

3.2. Cluster analysis of cytoarchitectonical differences and similarities in the prefrontal cortex

In order to quantitatively describe the inter-areal similarities and dissimilarities in cytoarchitecture as compared to inter-hemispheric differences, a hierarchical cluster analysis of the cytoarchitectonical profiles was performed (Fig. 13). Neighboring and more distant cortical areas were included (see *Material and Methods*).

The inter-hemispheric differences in cytoarchitecture of each of the selected areas were smaller than the inter-areal differences with the notable exception of the Broca areas 44 and 45. Only the latter two areas show a larger inter-hemispheric than inter-areal difference in cytoarchitecture, indicating lateralization. Area Fo1 was more similar to BA 12 and Fo2 to Fo3 (Fig. 13). Furthermore, Fo1 and BA12 are found together with the two frontopolar areas Fp1 and Fp2 on the

same major branch of the cluster tree, indicating a higher similarity between these four areas compared to Fo2 and Fo3. A clear difference could be found between the medial orbitofrontal areas and the lateral orbitofrontal area BA47. All cingulate areas cluster together, as do both areas of the Boca region (Fig. 13).

3.3. Intersubject variability

Probabilistic cytoarchitectonical maps of Fo1, Fo2 and Fo3 were computed in the anatomical MNI reference space (Figs. 14 and 15). The continuous probability maps demonstrate the intersubject variability of the position and extent of the cytoarchitectonically identified areas of the mOFC. In contrast, the MPMs represent a contiguous, non-overlapping parcellation of the OFC (Fig. 8). The MPM is not just a schematic or ‘typical’ map as in classical architectonical studies, but reflects the most likely area in each voxel of the MNI reference brain in stereotaxic space based on the present sample of 10 post-mortem brains.

The coordinates of the centers of gravity of the continuous probability maps (Figs. 14–15) as well as of the maximum probability maps (Fig. 8) are shown in Table 2, separately for right and left hemispheres. A good correspondence of stereotaxic coordinates of the centers of gravity is found between both the continuous probabilistic maps and their representations in the MPMs (Table 2).

The absolute volumes of all three OFC areas show a considerable intersubject variability both in female and male brains (Table 3). The absolute volumes of Fo1 and Fo2 vary a

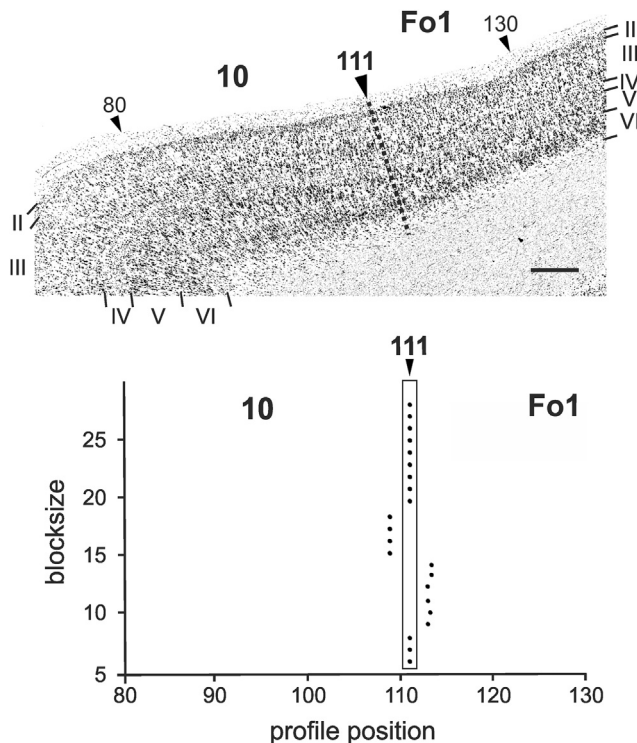


Fig. 7 – Border between areas Fo1 and BA10. Top: Region of interest in a cell body stained section through the rostral part of mOFC. Roman numerals indicate cortical layers, Arabic numerals indicate GLI profile positions, large arrowhead at position 111 marks the position of a significant ($p < .05$) maximum of the Mahalanobis distance, i.e., the cytoarchitectonical border between areas Fo1 and BA10. Bottom: Position (abscissa) of the significant maximum of the Mahalanobis distance plotted against block size (ordinate). Vertical frame corresponds to the accepted anatomical border. For details, see Material and Methods. Scale bar: 500 μ m.

factor of 1.6–2.1 in the left or right hemispheres, whereas the volumes of Fo3 vary by a factor of 1.2–1.5. We found no significant inter-hemispheric or sex differences in the volumes of Fo1, Fo2 or Fo3 using a permutation test which includes normalization for differences in total brain size and Bonferroni correction for multiple testing.

4. Discussion

4.1. Intersubject variability and its consequence for mapping

Previous maps of the human OFC differ considerably from each other regarding the number of cortical areas, their shape and relationship to macroscopical landmarks. The differences have various reasons. Some of the maps rely exclusively on studies of Nissl stained sections (Beck, 1949; Brodmann, 1909, 1910; von Economo & Koskinas, 1925; Mackey & Petrides, 2009; Ngowyang, 1934; Sarkisov et al., 1949; Uylings et al., 2010), whereas others use myelin stained sections (Strasburger,

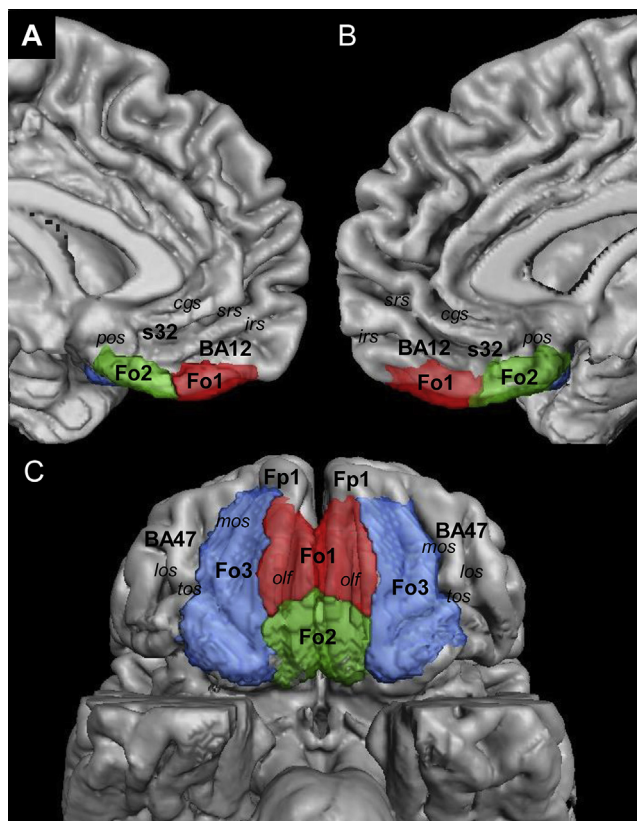


Fig. 8 – Maximum probability maps of cytoarchitectonically defined areas Fo1–Fo3 in the mOFC. A and B left and right mesial hemispheric surfaces, respectively. C ventral hemispheric surface. The position of adjacent areas, namely frontopolar area Fp1 (Bludau et al., 2014), BA12, lateral orbitofrontal BA47 (Brodmann, 1910), and cingulate area s32 (Palomero-Gallagher et al., 2008) is indicated. cgs cingulate sulcus, Fo1–Fo3 areas of the medial orbitofrontal cortex, irs inferior rostral sulcus, los lateral orbital sulcus, mos medial orbital sulcus, olfc olfactory cortex, olf olfactory sulcus, pos parolfactory sulcus, srs superior rostral sulcus.

1937; Vogt & Vogt, 1919), compare Nissl and myelin stained sections (Sanides, 1962), or are based on combined Nissl, myelin and immunohistochemical observations (Hof et al., 1995; Öngür & Price, 2000). These different staining methods may explain the differences in the number of identified areas. However, differences remain even if studies use a comparable combination of cyto- and myeloarchitecture as well as immunohistochemical staining (Hof et al., 1995; Öngür & Price, 2000). Apparently, the results are particularly dependent on the specific subjective weighting of the different microscopical criteria observed by different observers.

One example for “weighting” of cytoarchitectonical features is the usage of the criterion “agranular” (no layer IV visible), “dysgranular” (thin layer IV, less cell dense than in granular cortex), or “granular” (clearly visible and cell dense layer IV) between different reports. E.g., Hof et al. (1995) reported an agranular architecture in the caudal part of the gyrus rectus (their region PM; Fig. 1H), but Mackey and Petrides

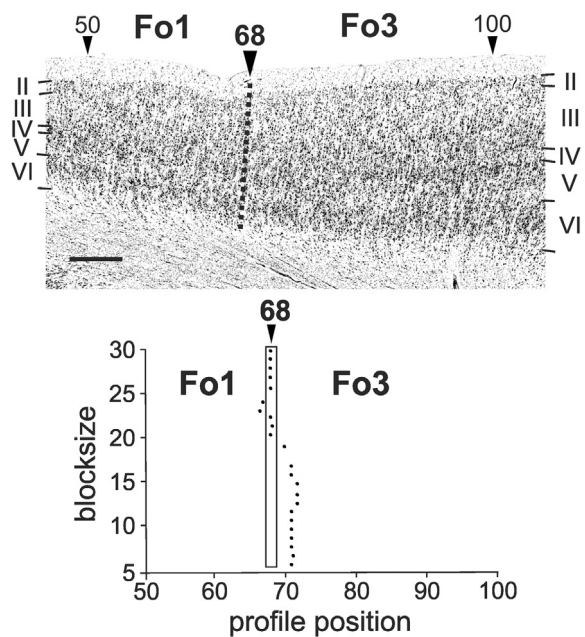
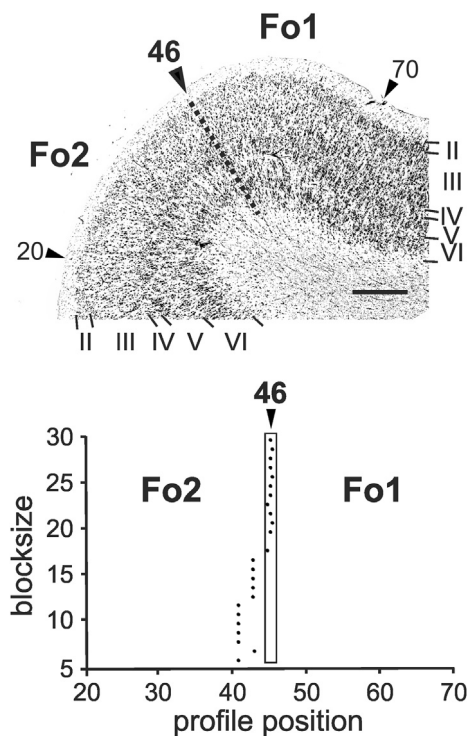
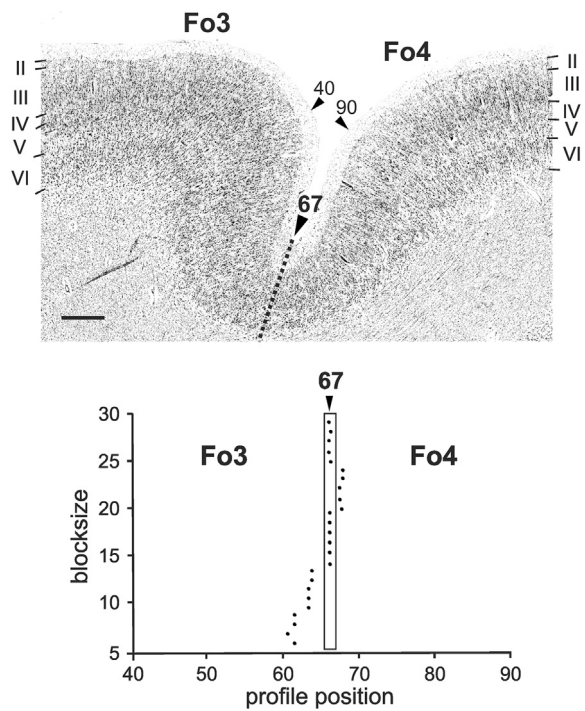
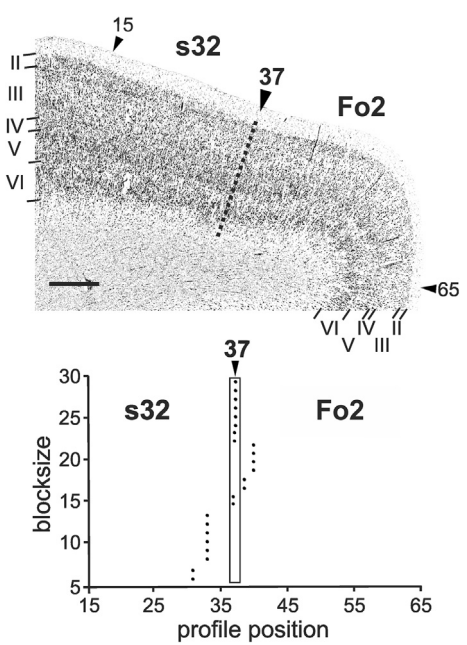


Fig. 9 – Border between areas Fo1 and Fo2. For further explanations see Fig. 7.

(2009) reported an “almost agranular” to dysgranular architecture in their areas 14c and 14r (Fig. 1F), and Öngür et al. (2003) described a dysgranular appearance of their area 14r (Fig. 1G). Since these terms indicate quantitative aspects of layer IV, i.e., density of granular cells, Mackey and Petrides (2009) explained the inconsistencies between previous

reports by the lack of quantitative data. We completely agree with their statement, as the transitions from agranular and dysgranular, or from dysgranular to granular are usually not abrupt. Even between the definitely agranular primary motor cortex and the extremely granular primary somatosensory cortex, area 3a is interleaved, which shows a mixture of agranular motor and granular sensory architecture (Zilles &



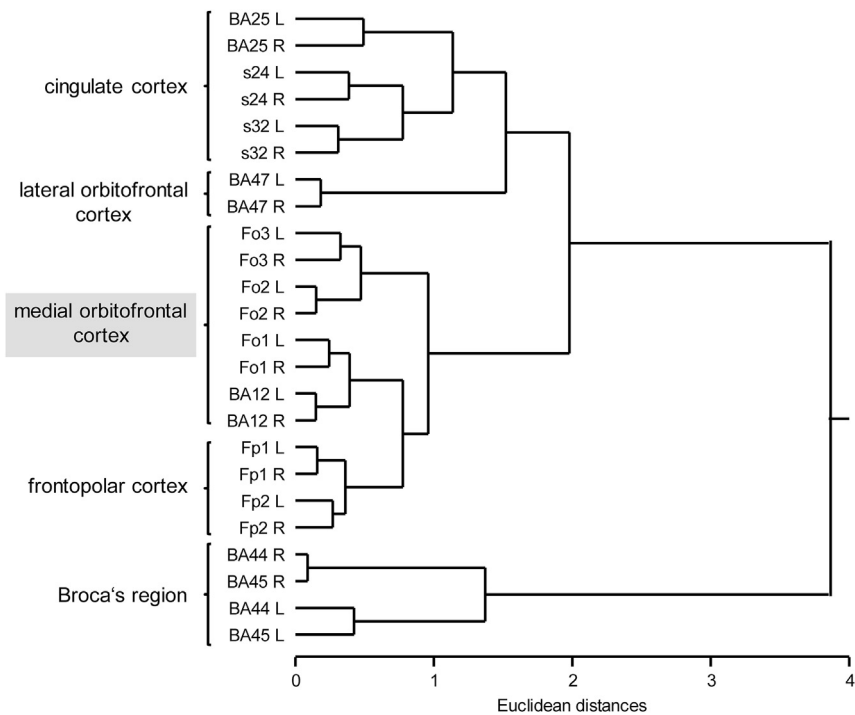


Fig. 13 – Hierarchical cluster analysis (Ward linkage, Euclidean distances) of 22 cytoarchitectonically defined areas of the frontal cortex. The Euclidean distance (Distances, x-axis) is based on features, which characterize the shape of the GLI profiles of an area (see Material and Methods). The hierarchical cluster analysis demonstrates the higher cytoarchitectonical similarity between the three mOFC areas as compared to all other frontal areas. It supports the principal segregation between the medial part of the OFC comprising areas Fo1–Fo3 and its lateral part with Fo4.

Amunts, 2011). The introduction of quantification and statistical testing is a solution, since it provides objective criteria to define areal borders independent from the more qualitative judgments of the observers and thus establishes reproducible maps.

A step towards an objective cytoarchitectonical description of OFC areas was already made by exploiting quantitative data mainly from layers IV and Va (Mackey & Petrides, 2009). The data were not used, however, for an observer-independent definition of areal borders, as those were nonetheless defined by visual inspection. Therefore, we have revisited the medial OFC with a quantitative cytoarchitectonic mapping procedure in which the definition of areal borders is based on a statistically testable method (Amunts & Zilles, 2001; Schleicher et al., 1999, 2005; Zilles & Amunts, 2010; Zilles et al., 2002).

The procedure of the present study enables the observer-independent detection and the statistical testing of the significance of areal borders by measuring tightly spaced laminar GLI profiles throughout the cortical width and along the cortical ribbon. Each profile represents layer-dependent changes of volume proportions of cell bodies at high spatial resolution. The GLI is not an abstract feature, but rather represents the most widely used and important cytoarchitectonical feature, i.e., the volume density of cell bodies (Wree et al., 1982). Moreover, an observer-independent definition of areal borders was achieved by statistical testing of the differences between pairs of neighboring groups of profiles (Schleicher et al., 1998, 1999, 2000, 2005), which are

moved along the cortical ribbon by a sliding window-like procedure. This approach is particularly useful for the parcellation of the OFC and the adjoining prefrontal cortex, since the architectonical differences between these homotypical isocortical areas of the orbitofrontal and prefrontal cortex cannot be characterized by unique markers, like area-specific cell types (e.g., the Betz cells in the primary motor cortex), or typical cortical layering (e.g., Gennari stripe in the primary visual cortex). The Mahalanobis distance, which is a multivariate distance measure between the feature vectors of immediately adjacent groups of GLI-profiles, quantifies the cytoarchitectonical differences within and between areas (Fig. 2). Within an area, the distances show in- and decreases, which can be interpreted as “noise” or as indicators of local fluctuations in cytoarchitecture possibly caused by patch-like distributions of input from various sources to a cytoarchitectonic area (Goldman-Rakic, 1984, 1995; Goldman-Rakic & Schwartz, 1982). However, at the borders between two areas, the fluctuations reach significant maxima (e.g., positions 47, 261, and 370 in Fig. 2). These maxima must fulfill two conditions before they can be interpreted as indicators of a cytoarchitectonic border: (i) they must be identified at the same or nearly the same position independent of the block size of the profiles in one brain section, and (ii) they must be found at a comparable position in neighboring sections of the serially sectioned brain. The present study shows that those significant maxima of the Mahalanobis distances provide a consistent delineation of three mOFC areas in all ten brains studied.

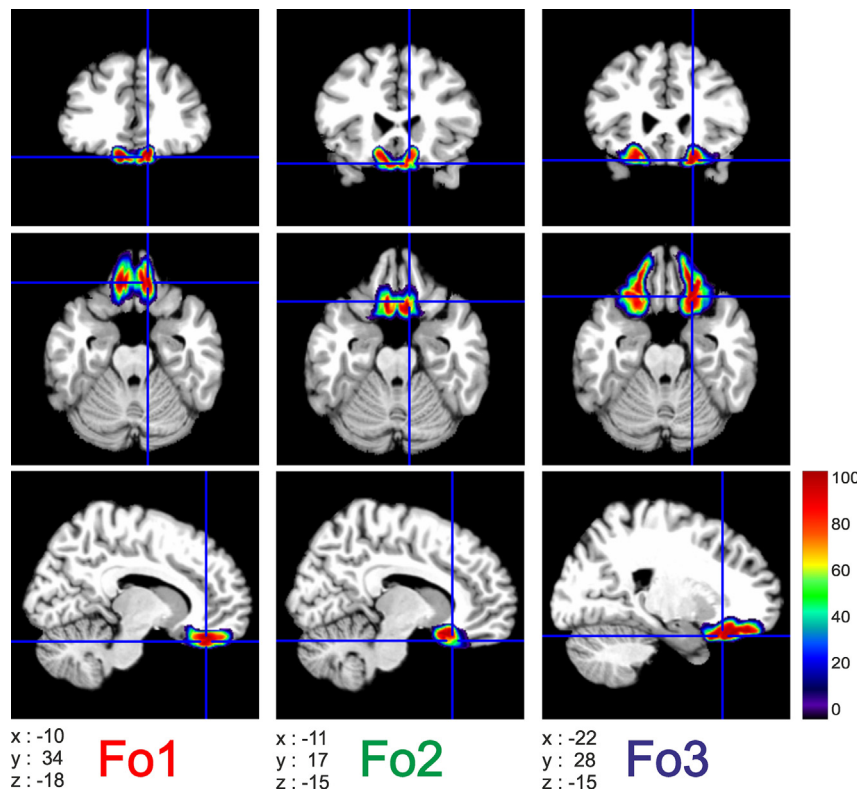


Fig. 14 – Continuous probability maps and stereotaxic coordinates of the areas Fo1–Fo3 in representative coronal (upper part), horizontal (middle part), and sagittal (lower part) sections. Color map encodes low probabilities in dark blue (one out of ten brains) up to high probabilities in dark red (ten out of ten brains). Stereotaxic location of the sections is given in the anatomical MNI space (Amunts et al., 2005). The origin of the original MNI reference space is located 4 mm more caudally (y-axis) and 5 mm more dorsally (z-axis) than that of the anatomical MNI space.

In the present observation, we use cell body stained sections exclusively, because this method can be easily performed in serial sections of complete human brains, which enables an overview over a large region of neighboring areas and registration to the MR volumes of the respective brains and to a stereotaxic reference space. We are aware of the possibility that maps based on a single staining technique can be further differentiated by delineations based on other staining techniques like immunohistochemistry (e.g., in the case of the mOFC) (Hof et al., 1995; Öngür et al., 2003), or by multiple receptor autoradiography as shown in other brain regions (Palomero-Gallagher et al., 2009; Zilles & Amunts, 2010; Zilles, Bacha-Trams, Palomero-Gallagher, Amunts, & Friederici, 2015; Zilles, Palomero-Gallagher, & Schleicher, 2004). Although multimodal mapping of cortical regions relying on multiple visualization techniques is necessary for a deeper understanding of the structural organization, the relation between the different unimodal maps can only be understood if each map is founded on a reliable and reproducible parcellation method.

A considerable intersubject variability of the OFC is already found at the macroanatomical level (Chiavaras & Petrides, 2000). Four major sulci (olfactory, medial, lateral and transverse orbital sulci) are commonly identified in the OFC (Fig. 8). The sulci macroscopically often look like the letters 'H', 'K' or 'X' (Ono, Kubik, & Abernathay, 1990), and are supplemented by

highly variably sulcal branches (Chi et al., 1977; Chiavaras et al., 2001).

The mOFC areas have relatively constant spatial relations to the sulcal landmarks, but sulcal fundi or other macroscopical landmarks in each individual brain do not precisely predict the localization of their borders as shown by the probability maps (Fig. 15). Although the interindividual variability of the extent and position of cytoarchitectonically defined areas may partly explain the differences between existing parcellation schemes, this aspect has rarely been taken into account in classical brain mapping studies. In contrast, the present maps (Figs. 8, 14 and 15) are not schematic drawings of cortical surface representations, but reflect the intersubject variability of each area by providing continuous and maximum probability maps. A further advantage of the present mapping in serially sectioned, complete human brains, which were MR scanned prior to sectioning and further histological processing, is the possibility to register cortical areas and their borders in 3D stereotaxic space. Therefore, these maps can be used as an anatomical reference for the interpretation of functional imaging data (Amunts & Zilles, 2001; Eickhoff et al., 2005, 2006, 2007).

The variability in position and extent of mOFC areas revealed by the probabilistic maps is further supported by the volumetric analysis of the size of the medial orbitofrontal areas in our sample (Table 3). The volumes of areas Fo1–Fo3

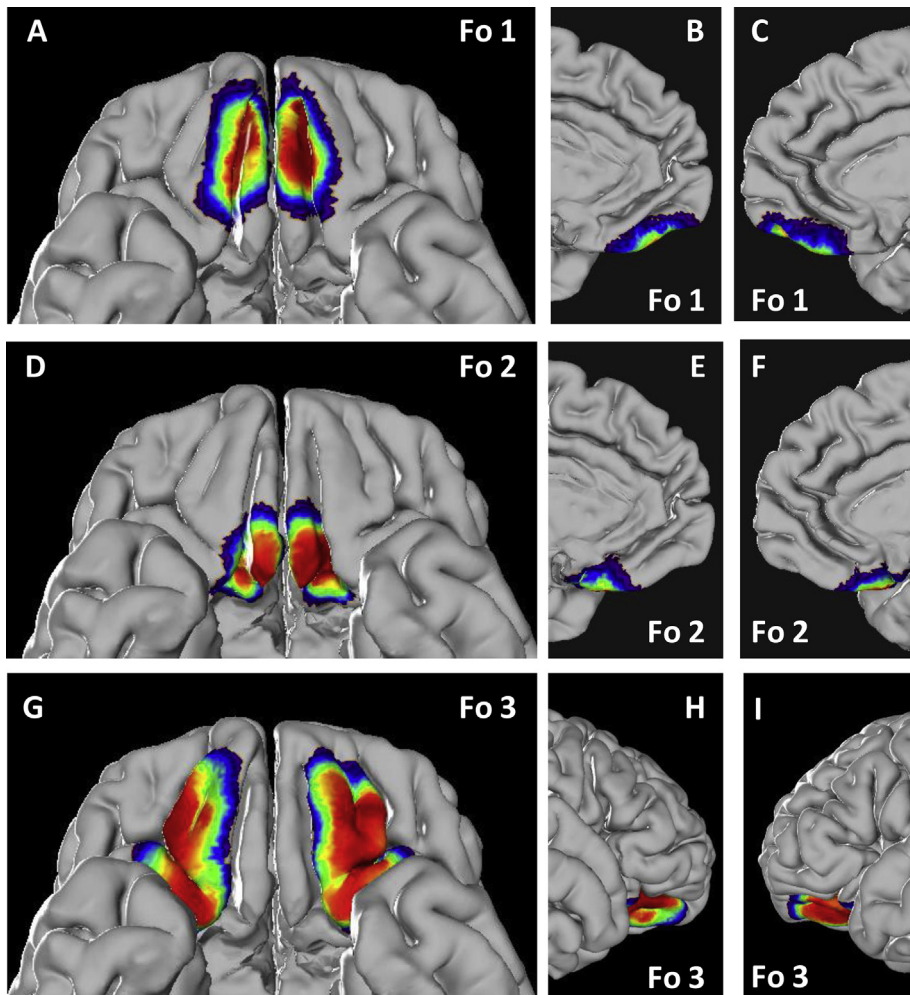


Fig. 15 – Continuous probability maps of areas Fo1–Fo3 projected to the surface. A, D, G ventral surface of the frontal lobe, B–C and E–F mesial views, H–I oblique view on the lateral surface of the reference brain.

vary by the factor 1.2–1.6 (with the only exception of area Fo2 (factor 2.1) in the right hemisphere of male brains). However, the variability in volume of these areas is much lower than those of areas 44 and 45 of the Broca region (Amunts et al., 1999) or areas in the inferior parietal lobule (Caspers et al., 2008), which vary by factors approximately three to five times higher. This result indicates that the interindividual variability is not a consequence of the variability of total brain volume, but has to be taken into account for each area separately. Its functional consequence remains a topic of further studies, and may be a correlate of functional specialization (Amunts et al., 2004).

We could not find significant differences between the volumes of male and female mOFC areas if the absolute volumes were normalized by total brain weights. Gur, Gunning-Dixon, Bilker, and Gur (2002) report a larger volume of the “orbital frontal” cortices in female than in male brains, but their region which comprises the “orbital frontal” cortex includes a much larger variety of cytoarchitectonical areas, i.e., parts of BA10, cingulate cortex, and medial and lateral orbital cortex. However, it must be noted, that we examined only ten postmortem brains, whereas Gur et al. (2002) studied 116

subjects *in vivo* using MRI. Therefore, the lack of gender differences in our study must be interpreted with caution because of the small sample size.

4.2. Comparisons with previous maps of the human OFC

In the existing maps of the OFC various nomenclatures are used: a numerical system (Fig. 1A, D, E, G) derived from Brodmann's map (1909), topographically arranged letter systems by von Economo and Koskinas (1925; Fig. 1B) and Hof et al. (1995; Fig. 1K), a numerical system (Fig. 1F, L) based on Walker's (1940) map on macaque brains, and a numerical system (Fig. 1C, H, I, J) proposed by Vogt and Vogt (1919).

4.2.1. Cytoarchitectonic maps

It is widely accepted that areas 11–14 represent OFC in the macaque cortex (Carmichael & Price, 1994, 1995; Mackey & Petrides, 2010; Petrides & Pandya, 1994), but the situation is less clear in the human brain as made obvious by the differences between the various maps (Brodmann, 1909, 1910; von Economo & Koskinas, 1925; Hof et al., 1995; Mackey &

Table 2 – Coordinates of the centres of gravity of continuous probability maps (PMap) and corresponding maximum probability maps (MPM) of areas Fo1–Fo3 based on 10 brains in anatomical MNI space. L left hemisphere, R right hemisphere. aMNI anatomical MNI space (Amunts et al., 2005), MNI original MNI space (Collins et al., 1994).

		PMap centre of gravity (L)			PMap centre of gravity (R)		
		x	y	z	x	y	z
Fo1	aMNI	-9	35	-19	10	35	-19
	MNI	-9	39	-24	10	39	-24
Fo2	aMNI	-10	18	-17	10	17	-17
	MNI	-10	22	-22	10	21	-22
Fo3	aMNI	-22	29	-16	22	28	-17
	MNI	-22	33	-21	22	32	-22
		MPM centre of gravity (L)			MPM centre of gravity (R)		
		x	y	z	x	y	z
Fo1	aMNI	-9	35	-19	10	35	-19
	MNI	-9	39	-24	10	39	-24
Fo2	aMNI	-9	18	-17	10	17	-17
	MNI	-9	22	-22	10	21	-22
Fo3	aMNI	-22	29	-16	22	28	-17
	MNI	-22	33	-21	22	32	-22

Petrides, 2009, 2010; Ngowyang, 1934; Öngür & Price, 2000; Sanides, 1962; Sarkisov et al., 1949; Strasburger, 1937; Uylings et al., 2010; Vogt & Vogt, 1919) (see also Fig. 1). Brodmann (1909) never identified areas 13 and 14 in the human brain. Both areas are parts of his insular region in *cercopithecus* and lemur brains. Brodmann (1909) explicitly described area 13 as a cortical area with a distinct inner granular layer and located behind the central sulcus of the monkey insular cortex, whereas area 14 is agranular and found in front of this sulcus. Walker (1940), however, used the labels 13 and 14 to identify two cortical areas located in the macaque OFC, and Beck (1949), Öngür et al. (2003) and Mackey and Petrides (2009, 2010) adopted this numerical system. Thus, their areas 13 and 14, which truly belong to the human and macaque OFC, should not be considered equivalent to Brodmann's (1909) areas BA13 or BA14 of the monkey insular cortex. Furthermore, Öngür et al. (2003), Mackey and Petrides (2009, 2010) and Paxinos, Huang, and Toga (2000) combined the Walker-nomenclature and that of Brodmann (1909) by

introducing terms like 47(12), 47/12l, 47/12m, 47/12o, and 47/12r for areas lateral to their areas 11 and 13 (Fig. 1L). These hybrid terms indicate that Walker's area 12 of the monkey (Walker, 1940) can be considered homologue to human BA47 (Brodmann, 1909), as proposed by Petrides and Pandya (1994). Thus, areas 47/12r, 47/12l and 47/12m of Öngür et al. (2003) belong to the lateral orbitofrontal region. Area 10 and its subdivisions extending partly on the orbital surface are part of the prefrontal cortex with a prominent layer IV, and represent its frontal pole region. Thus, area 10 is not included in the OFC.

4.2.2. Directed cytoarchitectonical gradations in the OFC

Based on a hypothesis of Vogt and Vogt (1919), Sanides (1962) was the first to elaborate on the existence of medial-to-lateral and posterior-to-anterior cytoarchitectonical gradients as important features of the structural differentiation in OFC. He proposed that the directions of these cytoarchitectonical “gradation” streams correlate with the directions of neocortical development during brain evolution. Starting points of both streams are the border regions of the evolutionary old paleo- and archicortex. He characterized the cytoarchitectonical changes along the gradation streams by the gradual changes of cytoarchitecture from one to the next area. The changes are most clearly visible in layers IIIC, IV and Va, and by the relationships of changes in cell size and density as well as in laminar width between the layers. Along the gradation streams, an increase in size of the layer IIIC pyramidal cells and in the width and density of granular cells in layer IV, as well as a parallel decrease in size of the layer V pyramidal cells are found (boxes in Fig. 16). Starting point of the medial-to-lateral stream is the periarchicortex on the mesial hemispheric surface; targets are the highly granular areas 60 and 61 of Sanides (1962) in the center of the orbital surface (Figs. 1J and 16). The posterior-to-anterior stream shows comparable gradual changes with the starting point in the parolfactory area of the paleocortex. The final target is BA10 (area 1 of Sanides, 1962; frontopolar areas Fp1 and Fp2 of Bludau et al., 2014). The isocortical area 6 of Sanides (1962; Fo2 in the present study) of this stream shows a dysgranular cytoarchitecture in its most posterior part, and the layer V pyramids are larger than the layer IIIC pyramids (see also box in Fig. 16 for area 6 and Fig. 6 for Fo2). The granular area area 4 of Sanides (1962; Fo1 in the present study) is an intermediate step on the way to BA10. A clear layer IV is visible in this area, and the layer IIIC pyramids are of equal size or larger than those in

Table 3 – Volumes [mm³] of medial orbitofrontal cortical areas Fo1–Fo3. Mean volumes (\pm SD) as well as maximal and minimal volumes of mOFC areas on the left and right hemispheres of male and female brains were measured in the reconstructed histological brain volumes ($n = 10$) prior to any spatial normalization. Volumes are given after individual correction for shrinkage during histological processing (Amunts et al., 2005).

	Fo1		Fo2		Fo3	
	Female	Male	Female	Male	Female	Male
Left	1262 \pm 317	1735 \pm 386	1387 \pm 275	1104 \pm 255	2732 \pm 407	3215 \pm 365
Minimum	972	1259	1035	930	2247	2752
Maximum	1755	2338	1714	1390	3301	3665
Right	1303 \pm 362	1841 \pm 386	1276 \pm 244	1097 \pm 269	2613 \pm 445	3141 \pm 216
Minimum	965	1307	1073	685	2199	2799
Maximum	1848	2166	1666	1382	3286	3301

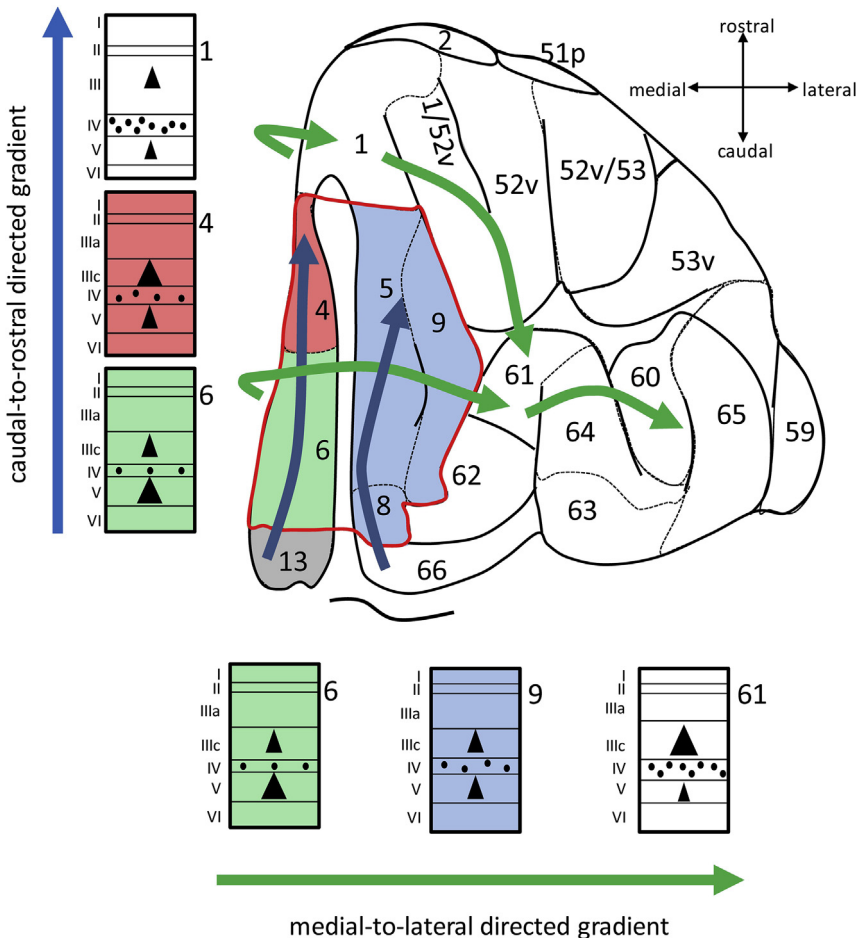


Fig. 16 – The “gradation” theory of [Sanides \(1962\)](#) applied to the mOFC areas. Blue arrows indicate the posterior-to-anterior directed gradation stream, green arrows the medial-to-lateral gradation stream of cytoarchitectonic differentiation. The major cytoarchitectonic features in layers IIIC, IV and V are schematically illustrated for selected areas 1, 4, 6, 9 and 61 of the Sanides map in the boxes. Arabic numerals label the cyto- and myeloarchitectonically defined areas after [Sanides \(1962\)](#). The approximate extensions of the mOFC areas are marked in red (Fo1), green (Fo2) and blue (Fo3). The red contour indicates the extent of mOFC.

layer V (see also box in Fig. 16 for area 4 and Fig. 6 for Fo1). In areas Fp1 and Fp2 (frontopolar cortex of Bludau et al., 2014) layer IV is much wider and more densely packed compared to Fo1. Furthermore, the pyramidal cells in layer III are larger than those in layer V (see also box in Fig. 16 for area 1 of [Sanides, 1962](#); which is part of BA10). The granular area Fo3 represents a step on the way to areas 60 and 61 of Sanides, which are located in the LOFC region (Fig. 16). The pyramidal cells in layer IIIC are slightly larger than those in layer V of Fo3 (Fig. 6). The packing density of granular cells in layer IV is lower in areas 5 and 9 (parts of Fo3) than in areas 60 and 61 ([Sanides, 1962](#)). These relative changes in size of the pyramidal cells between layers III and V as well as the width and density of granular cells in layer IV emphasized by [Sanides \(1962\)](#) in his gradation hypothesis match the present observations. Thus, the observer-independent definition of areal borders led to a parcellation, which reflects the gradation streams, and provides insight into the underlying developmental principles of the regional differentiation in human mOFC. The hierarchical cluster analysis (Fig. 13) of the

cytoarchitecture of the mOFC areas Fo1-Fo3 and various pre-frontal, language, and subgenual cingulate areas further supports the notion of [Sanides \(1962\)](#), that the areas of mOFC are cytoarchitectonically segregated from those of LOFC.

4.2.3. Myeloarchitectonic maps

Myeloarchitectonical studies seem to provide more detailed parcellations compared to cytoarchitectonical observations. In the mOFC, five to six isocortical areas were delineated in the myeloarchitectonical studies by [Vogt and Vogt \(1919; Fig. 1H: areas 4–9\)](#) and [Strasburger \(1937; Fig. 1I: areas 4 + 6, 5, 8, 9, 11\)](#). Areas 13, 14 and 7 + 14 of [Vogt and Vogt \(1919\)](#) are areas of the transition between iso- and allocortex, and are not included in the homotypical isocortex of the mOFC. As mentioned above, [Strasburger \(1937\)](#) could not find area 7 of [Vogt and Vogt \(1919\)](#), although both studies used the same myelin staining. Strasburger's finding was later confirmed by Hopf (1956), who re-analyzed both brains studied by [Vogt and Vogt \(1919\)](#) and [Strasburger \(1937\)](#). In cytoarchitectonical studies, Brodmann (Fig. 1A) identified one (BA11; [Brodmann, 1909](#)) or two (BA11

and BA12; Brodmann, 1910) homotypical isocortical areas in the mOFC. Sarkisov et al. (1949) also identify two areas (Fig. 1E: areas 11 and 12; the latter area is located on the mesial surface of the hemisphere and thus not visible in Fig. 1E), whereas other authors found more areas in this region. von Economo and Koskinas (1925; Fig. 1B: areas F_G, parts of F_E, F_{Er}, and F_F) and Uylings et al. (2010; Fig. 1G: areas 11, 12, 47 m¹, 47 m²) report four areas, and Beck (1949; Fig. 1D: area recta anterior, area recta posterior, areas t1, t2, 11, and 13) and Ngowyang (1934; Fig. 1C: areas 4–9) describe six areas.

The combined cyto- and myeloarchitectonical study of mOFC by Sanides (1962; Fig. 1J: areas 4–6, 9) describes five areas. The combined cytoarchitectonical, histochemical (acetylcholinesterase), and immunohistochemical (antibodies against neuronal cell bodies, parvalbumin, neurofilament protein) map of Öngür et al. (2003) displays eight cortical areas in the mOFC (Fig. 1L: areas 11m, medial part of 11l, 13a, 13b, 13m, 13l, 14r and 14c), but a comparably multimodal study by Hof et al. (1995; Fig. 1K: areas SO, AM, PM) shows only three areas.

In conclusion, staining techniques may influence the number of areas in mapping studies, but do not completely explain the differences between maps, because the number of identified areas also varies between observations using the same staining method, i.e., the same structure selectivity. Therefore, objective, i.e., statistically testable methods for the definition of areal borders are necessary to determine a cortical area. The difference in number of cortical areas between studies based on different staining techniques, however, is not contradictory *per se* as long as areas of a more detailed parcellation are a subset of a unique area defined in a less detailed map. In this case, both maps can be tiled upon each other without any controversies. E.g., areas 13a, 13b, 14c, and 14r, of the more detailed parcellation based on

immunohistochemistry by Öngür and Price (2000) are completely contained within Fo2.

4.2.4. Comparison between architectonic maps

While keeping in mind these differences in nomenclature, the relationship of areas Fo1–Fo3 with sulcal landmarks enables the identification of putative homologies with areas in previously published maps (Table 4). For area Fo1, matches are found with area F_G of von Economo and Koskinas (1925), area 4 of Vogt (1910), Vogt and Vogt (1919), Ngowyang (1934), Hopf (1956), and Sanides (1962), area AM of Hof et al. (1995), and area 11m of Öngür et al. (2003). Fo1 comprises the area recta anterior and area t1 of Beck (1949) and the combined area 4 + 6 of Strasburger (1937). For area Fo2, best matches are found with area FH of von Economo and Koskinas (1925), area 11 of Strasburger (1937) and Hopf (1956), area recta posterior of Beck (1949), area 6 of Sanides (1962), and area PM of Hof et al. (1995). Additionally, Fo2 comprises areas 6 and 7 of Vogt (1910), Vogt and Vogt (1919) and Ngowyang (1934), and areas 13a, 13b, 14c and 14r of Öngür et al. (2003). In case of area Fo3, the best match is found with area 47 m² of Uylings et al. (2010). Fo3 comprises areas 5, 8, and 9 of Vogt (1910), Vogt and Vogt (1919), Ngowyang (1934), Strasburger (1937), Hopf (1956) and Sanides (1962), as well as areas 11, 13 and t2 of Beck (1949). A comparison with the maps of Brodmann (1909, 1910) and Sarkisov et al. (1949) shows that their area 11 comprises areas Fo1, Fo2 and Fo3.

In conclusion, we can state, that in most cases areas Fo1–Fo3 either match previously delineated areas, or are subdivisions of such areas, or each of our areas was further subdivided in previous maps. We think that only one case (Öngür et al., 2003) may disagree with our map of the medial OFC, because their area 111 (Öngür et al., 2003) clearly encompasses a region medial and lateral of the medial orbital

Table 4 – Putative homologies between previous maps of OFC and areas Fo1, Fo2 and Fo3 of the present study.

	Fo1	Fo2	Fo3
Cytoarchitectonic maps			
Brodmann (1910)	Anteromedial part of 11	Posteromedial part of 11	Lateral part of 11
von Economo and Koskinas (1925)	F _G	F _H	Parts of F _E , F _F , and most medial part of F _{EF}
Ngowyang (1934)	4, Anterior part of 7	6, Posterior part of 7	5, 8, 9
Beck (1949)	Recta anterior and t1	Recta posterior	11, t2, 13
Sarkisov et al. (1949)	Anteromedial part of 11	Posteromedial part of 11	Lateral part of 11
Mackey and Petrides (2010)	Medial part of 11m and anteromedial part of 14r	Posteromedial part of 14r, medial part of 14c	Lateral parts of 11m, 14r, and 14c, medial part of 11
Uylings et al. (2010)	Anterior parts of 11 and 47m ¹	Posterior parts of 11 and 47m ¹	47m ²
Myeloarchitectonic maps			
Vogt (1910), Vogt and Vogt (1919)	4	6, 7	5, 8, 9
Strasburger (1937) and Hopf (1956)	4 + 6	11	5, 8, 9
Combined cyto- and myeloarchitectonic maps			
Sanides (1962)	4	6	5, 8, 9
Multimodal and connectivity maps			
Hof Mufson and Morrison (1995)	Medial part of AM	Medial part of PM	Lateral parts of AM and PM
Öngür Ferry and Price (2003)	11m	14r, 14c, 13a, 13b	13m, 13l, Medial part of 11l
Neubert et al. (2015)	11m	14m	13

sulcus (Fig. 1L), which seems to be the principal landmark separating the medial and lateral orbitofrontal cortices. Our hierarchical cluster analysis (Fig. 13) containing profiles extracted from the three medial orbitofrontal areas Fo1–Fo3 and from the lateral orbitofrontal area BA47, which are separated by the medial or intermediate orbital sulci. Areas Fo1–Fo3 cluster with BA12 and frontopolar areas Fp1 and Fp2, whereas BA47 is found in a separate cluster. The role of the medial orbital sulcus as an indicator of a cytoarchitectonical transition is also supported by the maps of Beck (1949) and Sarkissov et al. (1949), where this sulcus separates area 11 from area 47a and from 47¹, respectively. Also the myeloarchitectonic studies of Vogt and Vogt (1919) and Strasburger (1937) describe a principal transition in myeloarchitecture between the medial and lateral orbitofrontal areas at this sulcus. This is further supported in the combined cyto- and myeloarchitectonic observations of Sanides (1962) and the immunohistochemical study of Hof et al. (1995). Area BA12, which is not further delineated in the present work, is found on the mesial surface and was therefore not included in the study of the medial OFC *sensu strictu*, although its cytoarchitectonic organization is similar to that of area Fo1 (Fig. 13).

4.2.5. Architectonic maps and connectivity

Connectivity studies in the human brain using structural or functional MRI can contribute considerably to an independent mapping of cortical areas (Behrens et al., 2003; Catani & Thiebaut de Schotten, 2012; Eickhoff, Laird, Fox, Bzdok, & Hensel, 2014; Kahnt, Chang, Park, Heinze, & Haynes, 2012; Neubert et al., 2015; Smith et al., 2013). In the human brain, a recent meta-analysis has shown that the medial and lateral orbitofrontal cortices differ in their connectivity patterns (Zald et al., 2014).

A resting-state fMRI analysis of the connectivity of OFC provided a detailed map of the mOFC which is very similar to our cytoarchitectonic map (Kahnt et al., 2012). Most of their cluster 1 matches our areas Fo1 and Fo2, and their cluster 2 comparable to our area Fo3 if the six cluster model applied.

Cluster 1 was positively coupled with the medial prefrontal, posterior cingulate, medial and lateral temporal cortices, inferior parietal area 39, and the ventral striatum. Negative coupling was found with inferior parietal area 40 and lateral temporal areas. Cluster 2 showed positive coupling with the ventral striatum and basal forebrain and negative coupling with the posterior cingulate cortex and the midbrain.

In a more recent paper (Neubert et al., 2015), the segregation of the OFC in human and macaque brains was studied using fMRI and diffusion-weighted MRI. The most important result of this study for the present data is a stunning similarity of their mOFC parcellation with our map (Fig. 17). Their area 11m can be compared with our area Fo1, area 14m with Fo2, and their area 13 with Fo3 of the present study.

Fo1 is, therefore, preferentially functionally positively coupled with limbic areas (amygdala, hippocampus, posterior cingulate and retrosplenial cortices, ventral striatum) and the caudate. Fo2 showed again a strong coupling with limbic areas (amygdala, hippocampus, ventral striatum, hypothalamus), but not with the caudate, retrosplenial or posterior cingulate cortices. Also Fo3 is coupled with limbic areas (amygdala, hippocampus, ventral striatum, hypothalamus, temporal pole region, perirhinal and posterior cingulate cortices) and the posterior part of the inferior parietal lobule. In conclusion, all our areas of the mOFC are functionally positively coupled with limbic regions, but besides common coupling with amygdala, hippocampus and ventral striatum, differential preferences in functional connectivity can be assigned to each area.

4.3. Maps of the macaque OFC and their comparability with the present parcellation of human mOFC

Walker (1940) divided the macaque OFC into areas 10–14, where area 10 is found on the frontal pole, but extending into the orbital region of the other maps (Fig. 18B–D). His areas 11–14 and the caudal part of area 10 cover the orbital surface (Fig. 18A). The parcellation by Walker has since been widely used and further elaborated (Carmichael & Price, 1994; Mackey

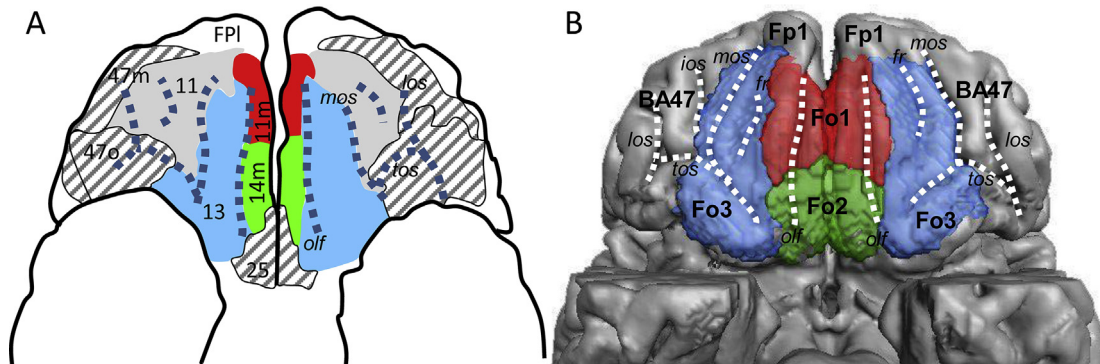


Fig. 17 – Comparison between the map of Neubert et al. (Neubert et al., 2015; A) and the present maximum probability map (B). Both maps are registered to the MNI brain. The sulci are labelled by thick dashed lines. 11 area 11, 11m area 11m, 13 area 13, 14m area 14m, 25 area 25, 47m area 47m, 47o area 47o, BA46 area 47 of Brodmann (1909), Fo1–Fo3 medial orbitofrontal areas 1–3, Fp1 frontopolar area Fp1 (Bludau et al., 2014), FPI lateral frontopolar area, fr sulcus fragmentosus, ios intermediate orbital sulcus, los lateral orbital sulcus, mos medial orbital sulcus, olf olfactory sulcus, tos transverse orbital sulcus.

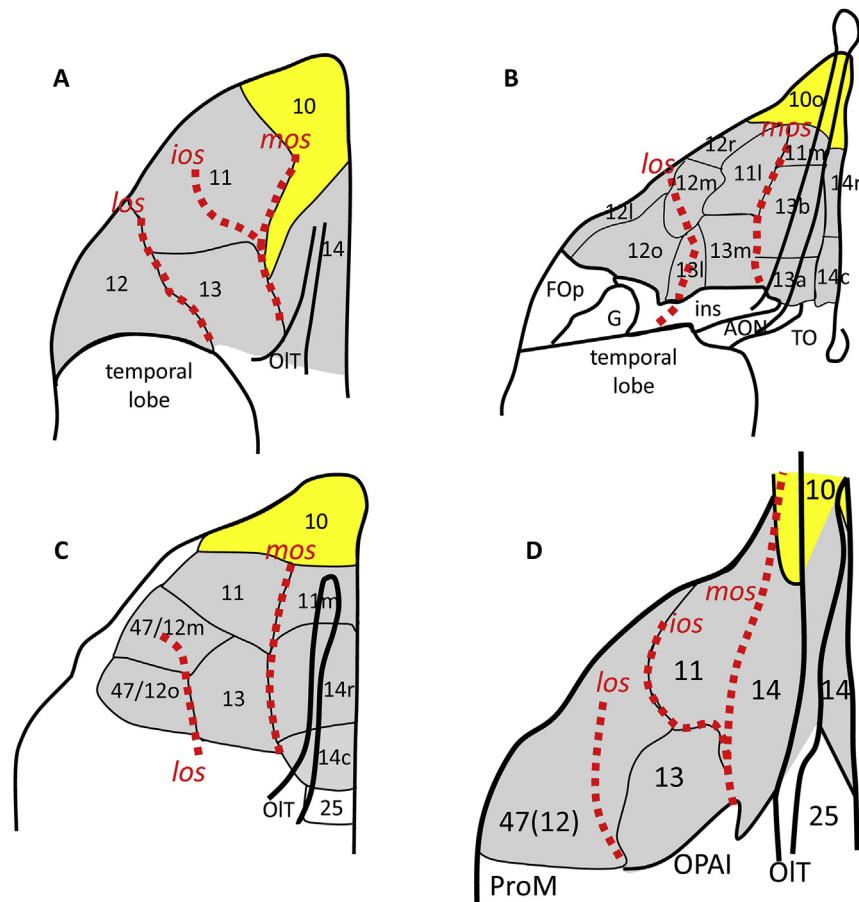


Fig. 18 – Maps of the orbitofrontal cortex in macaque monkeys. A [Walker \(1940\)](#), B [Carmichael and Price \(1994\)](#), C [Petrides and Pandya \(1994\)](#), D [Paxinos et al. \(2000\)](#). The map in D was reconstructed by the authors on the basis of the series of coronal sections given in [Paxinos et al. \(2000\)](#), and the labelling of sulci was added in A and C. Frontopolar area 10 is highlighted in yellow, OFC areas in gray. AON anterior olfactory nucleus; FOp frontal operculum; G gustatory cortex; ins insular cortex; los intermediate orbital sulcus; mos medial orbital sulcus; ProM area ProM; olf olfactory sulcus; OIT olfactory tract; OPAI orbital periallocortex; TO olfactory tubercle.

& Petrides, 2009; Paxinos et al., 2000). Carmichael and Price (1994; Fig. 18B) described the most numerous subdivisions of the OFC.

The various maps of the OFC in macaque monkeys seem to be similar (Fig. 18) at a first glance, but a closer examination reveals interesting differences (Table 5). The most obvious difference is the extreme caudal extension of the frontopolar area 10 in the map of [Walker \(1940\)](#); Fig. 18A) compared to the three other maps. Furthermore, area 11 of [Walker \(1940\)](#) extends much more laterally than in the maps of [Carmichael and Price \(1994\)](#); Fig. 18B) and [Paxinos et al. \(2000\)](#); Fig. 18D). Finally, the maps of [Walker \(1940\)](#), Mackey and Petrides (2010; Fig. 18C) and [Paxinos et al. \(2000\)](#) show an area 13 which does not extend medial to the medial orbital orbital sulcus, but is clearly located medial to this landmark in the map of [Carmichael and Price \(1994\)](#). Briefly, despite of the relatively low variability of the monkey brain, some conspicuous differences between the available maps have been reported in the literature. Therefore, a straightforward comparison between the cytoarchitectonic maps of all OFC areas in the monkey brain is difficult (Table 5) and probably requires a re-

mapping using multimodal and observer-independent methods.

The relationships between the position and extent of cytoarchitectonic areas and sulci, as well as the cytoarchitectonic structure of each area, are the basis for an interspecific comparison between human and monkey maps of the OFC in Table 6.

As stated above, the medial or intermediate orbital sulci are landmarks for the lateral border of the mOFC in the human and macaque brains. The medial orbital sulcus is also a consistent landmark for the lateral border of area 14 in the maps of the macaque OFC by [Walker \(1940\)](#); Fig. 18A), [Mackey and Petrides \(2010\)](#); Fig. 18C) and [Paxinos et al. \(2000\)](#); Fig. 18D), but not in that of [Carmichael and Price \(1994\)](#); Fig. 18B), where areas 11m, 13a and 13b medially adjoin this sulcus. Most probably, macaque area 14r of [Carmichael and Price \(1994\)](#) and [Mackey and Petrides \(2010\)](#) is part of our human Fo1, which also contains the area 11m of both authors. Area 11m seems to be included in macaque area 14 of [Paxinos et al. \(2000\)](#). Thus, area 14 of the latter author comprises our areas Fo1 and Fo2 (Table 6). Our area Fo2 is very similar to the caudal part of area

Table 5 – Comparison between cytoarchitectonic maps of OFC areas in the monkey brain based on localization and extent of cytoarchitectonic areas and their topographic relationships.

	Frontopolar region	I OFC	mOFC
Walker (1940)	Rostral part of 10	11 (Probably only lateral part) 12	Rostrolateral part of 13 Caudal part of 10, 11 (probably only medial part), caudomedial part of 13, 14
Carmichael and Price (1994)	10o	11l, 12m, 12r Lateral part of 11, medial part of 47/12m	13l Lateral part of 13 11m, 13a, 13b, 13m, 14c, 14r
Mackey and Petrides (2010)	10	47/12o, lateral part of 47/12m Rostromedial part of 47(12)	Medial part of 11, 11m, medial part of 13, 14c, 14r
Paxinos et al. (2000)	10	47/12l Caudolateral part of 47(12)	11, 13, 14 Caudomedial part of 47(12)

14 of [Walker \(1940\)](#) and [Paxinos et al. \(2000\)](#), as well as 14c of [Carmichael and Price \(1994\)](#) and [Mackey and Petrides \(2010\)](#). However, 13a of [Mackey and Petrides \(2010\)](#) is probably also part of our Fo2 in the human brain. Finally, the human area Fo3 best corresponds to the medial part of 11 and the caudo-medial part of 13 of [Walker \(1940\)](#) and [Mackey and Petrides \(2010\)](#) and areas 11l and 13m of [Carmichael and Price \(1994\)](#) as well as 11 and 13 of [Paxinos et al. \(2000\)](#). Compare [Figs. 17 and 18](#) and [Tables 5 and 6](#) for further details.

A comparative functional connectivity study in human and monkey brains revealed an interesting commonalities and differences between the mOFC maps and the functions of the areas in both species ([Neubert et al., 2015](#)). The probable homologs of Fo1–Fo3 in humans and monkeys were found to be positively functionally coupled with limbic regions, mainly amygdala, hippocampus, hypothalamus and ventral striatum. Beside these commonalities, however, various area-specific differences in connectivity with lateral prefrontal and inferior parietal areas as well as with areas in the intraparietal sulcus were found. It is presently not possible to decide whether these differences are caused by methodical issues (limited spatial resolution of structural and functional connectivity studies using MRI, uncertainties regarding comparisons between areas based only on architectonic criteria, variability of sulcal patterns within and between species and their significance as landmarks for architectonic areas), represent evolutionary developments, or could be interpreted as signs of “cultural recycling” ([Dehaene & Cohen, 2007](#)). The differences should, however, not obscure the similarities between the organization of the human and monkey mOFC and its implication in the limbic system. The overall similarity in connectivity and function and its mapping to three cortical areas ([Neubert et al., 2015](#)) is in accordance with our observations based on quantitative and statistically testable cytoarchitectonic analysis in the human brain and comparisons with previously published maps of human and macaque OFC.

4.4. Comparison between functional and cytoarchitectonical findings

In the present study, left-right differences in cytoarchitecture and volume that would exceed inter-areal differences are not found in the mOFC areas. This is in contrast to areas 44 and 45 of Broca's region, which show left-right differences in cytoarchitecture ([Fig. 13](#)) and volume ([Amunts et al., 1999](#)) as well as receptor expression ([Zilles et al., 2015](#)) that are larger than the inter-areal differences. Therefore, the functional lateralization of Broca's speech region has a parallel structural lateralization in size, cytoarchitecture and receptor expression differences, whereas the functional left-right differences reported for the whole OFC are not accompanied by inter-hemispheric differences in size and cytoarchitecture of the mOFC areas. There are only a few functional imaging studies which report inter-hemispheric differences in the OFC. Pronounced deficits in odor discrimination were found after lobectomy of the right OFC ([Zatorre & Jones-Gotman, 1991](#)). This finding of a functional lateralization in favor of the right OFC was later confirmed in PET studies using olfactory stimulation paradigms ([Zatorre, Jones-Gotman, Evans, & Meyer, 1992](#); [Zatorre, Jones-Gotman, & Rouby, 2000](#)). The reported

Table 6 – Comparison between cytoarchitectonic maps of mOFC areas in the monkey brain and the present parcellation in the human brain based on localization and extent of cytoarchitectonic areas and their topographic relationships.

Human areas in mOFC	Walker (1940)	Carmichael and Price (1994)	Mackey and Petrides (2010)	Paxinos et al. (2000)
Fo1	Caudal part of 10, rostral part of 14	11m, 13b, 14r	11m, 14r	Rostral part of 14
Fo2	Caudal part of 14	13a, 14c	14c	Caudal part of 14
Fo3	Medial part of 11, caudomedial part of 13	11l, 13m	Medial part of 11, caudomedial part of 13	11, 13

coordinates of the activation focus are found within area Fo1. Thus, amongst other functions, mOFC seems to be involved in higher-order olfactory processing. Right-handers show an asymmetry in cortical thickness in favor of the left IOFC during childhood, but a reverse in favor of the right hemisphere is reached by late adolescence (Shaw et al., 2009). Activation in a region comparable to the caudal part of Fo3 is higher in the left than right hemisphere during hedonic than during familiarity judgments of odor stimuli, whereas right Fo3 activation is highest during familiarity judgments but lowest during the detection (Royet et al., 2001). A similar lateralization in favor of the left Fo3 is found for emotional rating of visual and auditory stimuli (Royet et al., 2000). The mismatch between functional lateralization and the lack of structural/volume lateralization may be caused by the inevitably smaller sample size of cytoarchitectonic studies, which may not enable to detect minor volumetric differences between left and right hemispheres, or by a functional lateralization which must not necessarily lead to interhemispheric differences in volume, but can be based on differences in functional connectivity.

Functional neuroimaging studies of the human brain suggest a considerable regional heterogeneity of the OFC highlighting the principal functional division into the mOFC and IOFC, which matches the here described principal cytoarchitectonic division into the areas Fo1–Fo3 of the mOFC in contrast to BA47 of the IOFC (see Fig. 13). A meta-analysis (Kringelbach & Rolls, 2004) demonstrates this medio-lateral segregation with the mOFC being responsible for monitoring the reward value of different reinforcers (e.g., taste, touch, pain, olfactory, auditory and visual stimuli), whereas the IOFC is related to the evaluation of punishers with the consequence of changes in ongoing behavior. The positive correlation between activation and pleasure and reward elicited by music is found in the mOFC, particularly in the region corresponding to Fo3 (Blood & Zatorre, 2001; Blood et al., 1999). Pleasantness of taste and olfaction leads to activations in mOFC (de Araujo, Kringelbach, Rolls, & McGlone, 2003; de Araujo, Rolls, Kringelbach, McGlone, & Phillips, 2003; Gottfried, Deichmann, et al., 2002), i.e., our cytoarchitectonically identified areas Fo1–Fo3. Expectation of pleasant taste activates the region of Fo3 (O'Doherty, Dayan, et al., 2003; O'Doherty, Deichmann, Critchley, & Dolan, 2002). Also activity of the mOFC, particularly of a region corresponding to Fo3 is found during retrieval of positive memories (Schnider, Treyer, & Buck, 2000). Learning of pleasant olfactory stimuli is correlated with activity in the region of Fo3, whereas learning of unpleasant olfactory stimuli is correlated with activity in the IOCF (Gottfried, O'Doherty, et al., 2002).

Fo3 seems to be involved in various higher processing steps of olfaction. It is associated with valence of olfaction

independent of intensity (Anderson et al., 2003; Royet et al., 2001, 2000), pleasantness and intensity judgments odors (Zatorre et al., 1992, 2000), and hedonic and familiarity aspects of those stimuli (Royet et al., 2001). Additionally, Fo3 is activated by affective aspects of touch (Rolls, Kringelbach, et al., 2003), evaluation of pain, thermal intensity (Bantick et al., 2002; Craig, Chen, Bandy, & Reiman, 2000; Lorenz et al., 2003), and emotional evaluation of auditory stimuli (Frey & Petrides, 2000; Royet et al., 2000).

Passive viewing of beautiful faces or of happy facial expressions elicits activations in Fo2, Fo3 and other regions of the reward circuitry (Aharon et al., 2001; Gorno-Tempini et al., 2001; Iwase et al., 2002). It has been shown, that stimuli representing known objects evoke responses in the OFC (Chaumon, Kveraga, Barrett, & Bar, 2014). The mOFC seems to participate in the processing of the values of the visual stimuli in order to prepare appropriate reactions to visual information and informs the IOFC to send the visual predictions to the visual system (Chaumon et al., 2014). In this sense, the mOFC areas Fo1–Fo3 play a crucial role in a system reminiscent of the predictive coding hypothesis (Rao & Ballard, 1999). A more recent meta-analytic study also shows the medial-to-lateral segregation with the IOFC as part of a network involved in cognitive functions including language and memory, and the mOFC connected to the default mode network, as well as autonomic and limbic regions (Zald et al., 2014). Interestingly, comparable medial-to-lateral trends are described as micro-structural “gradations” by Sanides (1962) for the cyto- and myeloarchitectonical differentiation of the OFC in a study of the anatomy in the human frontal cortex.

The functional posterior–anterior distinction is based on the more anterior representation of complex or abstract reinforcers. Stimulation by the magnitude of virtual monetary reward leads to activity in a region comparable by its stereotaxic coordinates with our area Fo1 (O'Doherty et al., 2001). Activity elicited by abstract and rewarding reinforcers (e.g., beauty in a smile, O'Doherty, Winston, et al., 2003; hedonic aspects of smell, Rolls, Kringelbach, et al., 2003; Rolls, O'Doherty, et al., 2003; addictive behavior, Völlm et al., 2004; retrieval of words from positive context, Maratos, Dolan, Morris, Henson, & Rugg, 2001) are found at a site comparable to the anteriorly located area Fo1. Activation of a network including Fo1 was described (Rilling et al., 2002), which positively reinforces reciprocal altruism. Fo1 seems to be also involved in empathy (Farrow et al., 2001), decision making in conflict situations (Rogers et al., 1999), moral judgments in contrast to social judgments, which are correlated with activity in the IOFC (Moll, de Oliveira-Souza, Bramati, & Grafman, 2002, and the perception and attribution of emotion (Wicker, Perrett, Baron-Cohen, & Decety, 2003). More posterior

areas (Fo2 and central and posterior parts of Fo3) seem to represent primary reinforcers such as taste, satiety or pain (Craig et al., 2000; de Araujo, Kringelbach, Rolls, & McGlone, 2003; de Araujo, Rolls, et al., 2003; Kringelbach et al., 2003; Small, Zatorre, Dagher, Evans, & Jones-Gotman, 2001). This directed trend in functional diversity parallels the trend in cytoarchitectonic differentiation from the dysgranular posterior part of area Fo2 to the granular area Fo1 is found in the present observations.

A recent fMRI study (Neubert et al., 2015) demonstrated a strong functional coupling between the OFC and the ventromedial prefrontal cortex in both human and monkey brains, thus suggesting a role in a neural network subserving value-comparison and decision making (Neubert et al., 2015). Area 14m has been linked to decisions or attentional selection of choices. Category-dependent value signals were found in areas which most probably resemble Fo1 and Fo2 and are also connected with limbic areas (McNamee, Rangel, & O'Doherty, 2013). This argues for emotional and hedonic information processing, and may lead to an evaluation of a given stimulus in the context of the subject's internal state and external conditions.

5. Conclusions

Three cytoarchitectonical areas, Fo1, Fo2, and Fo3 were identified in the human mOFC using an observer-independent, quantitative cytoarchitectonic approach in a sample of 10 post-mortem brains. The present study provides the first cytoarchitectonical map of the mOFC, in which the significance of the borders between cortical areas was statistically tested. The cytoarchitecture of these areas differs significantly between each other, and from that of the surrounding frontopolar area, the anterior cingulate areas, and area BA47 of the IOFC. The volumes of the three mOFC areas do not show a significant hemispheric asymmetry.

The cellular differences between the mOFC areas are mainly found in the degree of differentiation in layers III, IV, and Va. The here observed directions of the differentiation gradients supports the “gradation stream theory” of Sanides (1962), which hypothesizes an increase in size of the pyramidal cells in layer III, an increase in width and granularity of layer IV, and a decrease of pyramidal cells in layer Va along a gradation stream from the allo- and periallocortex to the frontopolar and lateral prefrontal regions.

The probability maps show consistent relationships to sulcal landmarks with Fo1 and Fo2 located mainly medial of the olfactory sulcus, and Fo3 laterally bordered by the medial or intermediate orbital sulci. The probability maps of the mOFC areas in MNI space enable the anatomical localization of functional imaging data. To encourage the use of these probabilistic cytoarchitectonical maps for anatomical localization in functional imaging experiments, they were registered to the JuBrain atlas (<http://www.jubrain.fz-juelich.de/apps/cytoviewer/cytoviewer-main.php>), which is freely available, and can be used by means of the Anatomy toolbox (Eickhoff et al., 2005; www.fz-juelich.de/inm/inm-1/spm_anatomy_toolbox).

Conflict of interest statement

The authors have no conflict of interest to disclose.

Acknowledgments

This work was supported by the DFG (IRTG 1328, KA, SBE) as well as by the European Union Seventh Framework Programme (FP7/2007-2013) under grant agreement no. 604102 (Human Brain Project), and the Portfolio Theme “Supercomputing and Modeling for the Human Brain” of the Helmholtz Association, Germany (to KA and KZ).

REFERENCES

- Aharon, I., Etcoff, N., Ariely, D., Chabris, C. F., O'Connor, E., & Breiter, H. C. (2001). Beautiful faces have variable reward value: fMRI and behavioral evidence. *Neuron*, 32(3), 537–551.
- Amunts, K., Kedo, O., Kindler, M., Pieperhoff, P., Mohlberg, H., Shah, N. J., et al. (2005). Cytoarchitectonic mapping of the human amygdala, hippocampal region and entorhinal cortex: intersubject variability and probability maps. *Anatomy and Embryology (Berl)*, 210(5–6), 343–352.
- Amunts, K., Malikovic, A., Mohlberg, H., Schormann, T., & Zilles, K. (2000). Brodmann's areas 17 and 18 brought into stereotaxic space—where and how variable? *NeuroImage*, 11(1), 66–84.
- Amunts, K., Schleicher, A., Bürgel, U., Mohlberg, H., Uylings, H. B., & Zilles, K. (1999). Broca's region revisited: cytoarchitecture and intersubject variability. *Journal of Comparative Neurology*, 412(2), 319–341.
- Amunts, K., Schleicher, A., & Zilles, K. (2004). Outstanding language competence and cytoarchitecture in Broca's speech region. *Brain and Language*, 89(2), 346–353.
- Amunts, K., & Zilles, K. (2001). Advances in cytoarchitectonic mapping of the human cerebral cortex. *Neuroimaging Clinics of North America*, 11(2), 151–169.
- Anderson, A. K., Christoff, K., Stappen, I., Panitz, D., Ghahremani, D. G., Glover, G., et al. (2003). Dissociated neural representations of intensity and valence in human olfaction. *Nature Neuroscience*, 6(2), 196–202.
- de Araujo, I. E., Kringelbach, M. L., Rolls, E. T., & Hobden, P. (2003). Representation of umami taste in the human brain. *Journal of Neurophysiology*, 90(1), 313–319.
- de Araujo, I. E., Kringelbach, M. L., Rolls, E. T., & McGlone, F. (2003). Human cortical responses to water in the mouth, and the effects of thirst. *Journal of Neurophysiology*, 90(3), 1865–1876.
- de Araujo, I. E., Rolls, E. T., Kringelbach, M. L., McGlone, F., & Phillips, N. (2003). Taste-olfactory convergence, and the representation of the pleasantness of flavour, in the human brain. *European Journal of Neuroscience*, 18(7), 2059–2068.
- Bantick, S. J., Wise, R. G., Ploghaus, A., Clare, S., Smith, S. M., & Tracey, I. (2002). Imaging how attention modulates pain in humans using functional MRI. *Brain*, 125(Pt 2), 310–319.
- Barbas, H. (1992). Architecture and cortical connections of the prefrontal cortex in the rhesus monkey. *Advances in Neurology*, 57, 91–115.
- Barbas, H. (1993). Organization of cortical afferent input to orbitofrontal areas in the rhesus monkey. *Neuroscience*, 56(4), 841–864.

- Barbas, H. (2000). Complementary roles of prefrontal cortical regions in cognition, memory, and emotion in primates. *Advances in Neurology*, 84, 87–110.
- Barbas, H., & De Olmos, J. (1990). Projections from the amygdala to basoventral and mediodorsal prefrontal regions in the rhesus monkey. *Journal of Comparative Neurology*, 300(4), 549–571.
- Barbas, H., & Pandya, D. N. (1987). Architecture and frontal cortical connections of the premotor cortex (area 6) in the rhesus monkey. *Journal of Comparative Neurology*, 256(2), 211–228.
- Beck, E. (1949). A cytoarchitectural investigation into the boundaries of cortical areas 13 and 14 in the human brain. *Journal of Anatomy*, 83, 147–157.
- Behrens, T. E., Johansen-Berg, H., Woolrich, H. H., Smith, S. M., Wheeler-Kingshott, C. A., Boulby, P. A., et al. (2003). Non-invasive mapping of connections between human thalamus and cortex using diffusion imaging. *Nature Neuroscience*, 6(7), 750–757.
- Blood, A. J., & Zatorre, R. J. (2001). Intensely pleasurable responses to music correlate with activity in brain regions implicated in reward and emotion. *Proceedings of the National Academy of Sciences of the United States of America*, 98(20), 11818–11823.
- Blood, A. J., Zatorre, R. J., Bermudez, P., & Evans, A. C. (1999). Emotional responses to pleasant and unpleasant music correlate with activity in paralimbic brain regions. *Nature Neuroscience*, 2(4), 382–387.
- Bludau, S., Eickhoff, S. B., Mohlberg, H., Caspers, S., Laird, A. R., Fox, P. T., et al. (2014). Cytoarchitecture, probability maps and functions of the human frontal pole. *NeuroImage*, 93(Pt 2), 260–275.
- Brodmann, K. (1909). *Vergleichende Lokalisationslehre der Großhirnrinde in ihren Prinzipien dargestellt auf Grund des Zellbaues*. Leipzig (Germany): Barth.
- Brodmann, K. (1910). Feinere Anatomie des Großhirns. In M. Lewandowsky (Ed.), *Handbuch der Neurologie, Allgemeine Neurologie* (Vol. 1, pp. 206–307). Berlin (Germany): Springer.
- Carmichael, S. T., Clugnet, M. C., & Price, J. L. (1994). Central olfactory connections in the macaque monkey. *Journal of Comparative Neurology*, 346(3), 403–434.
- Carmichael, S. T., & Price, J. L. (1994). Architectonic subdivision of the orbital and medial prefrontal cortex in the macaque monkey. *Journal of Comparative Neurology*, 346, 366–402.
- Carmichael, S. T., & Price, J. L. (1995). Sensory and premotor connections of the orbital and medial prefrontal cortex of macaque monkeys. *Journal of Comparative Neurology*, 363(4), 642–664.
- Caspers, S., Eickhoff, S. B., Geyer, S., Schepers, F., Mohlberg, H., Zilles, K., et al. (2008). The human inferior parietal lobule in stereotaxic space. *Brain Structure and Function*, 212(6), 481–495.
- Catani, M., & Thiebaut de Schotten, M. (2012). *Atlas of human brain connections*. Oxford: Oxford University Press.
- Cavada, C., Company, T., Tejedor, J., Cruz-Rizzolo, R. J., & Reinoso-Suarez, F. (2000). The anatomical connections of the macaque monkey orbitofrontal cortex. A review. *Cerebral Cortex*, 10(3), 220–242.
- Chaumon, M., Kveraga, K., Barrett, L. F., & Bar, M. (2014). Visual predictions in the orbitofrontal cortex rely on associative content. *Cerebral Cortex*, 24(11), 2899–2907.
- Chi, J. G., Dooling, E. C., & Gilles, F. H. (1977). Gyral development of the human brain. *Annals of Neurology*, 1(1), 86–93.
- Chiavaras, M. M., LeGoualher, G., Evans, A., & Petrides, M. (2001). Three-dimensional probabilistic atlas of the human orbitofrontal sulci in standardized stereotaxic space. *NeuroImage*, 13(3), 479–496.
- Chiavaras, M. M., & Petrides, M. (2000). Orbitofrontal sulci of the human and macaque monkey brain. *Journal of Comparative Neurology*, 422(1), 35–54.
- Craig, A. D., Chen, K., Bandy, D., & Reiman, E. M. (2000). Thermosensory activation of insular cortex. *Nature Neuroscience*, 3(2), 184–190.
- Dehaene, S., & Cohen, L. (2007). Cultural recycling of cortical maps. *Neuron*, 56(2), 384–398.
- Dixon, W. J. (1988). *BMDP statistical software manual*. Berkeley: University of California Press.
- Eberstaller, O. (1890). *Das Stirnhirn. Ein Beitrag zur Anatomie der Oberfläche des Grosshirns*. Wien (Austria): Urban & Schwarzenberg.
- von Economo, K., & Koskinas, G. (1925). *Die Cytoarchitektonik der Hirnrinde des erwachsenen Menschen*. Wien (Austria): Springer.
- Eickhoff, S. B., Heim, S., Zilles, K., & Amunts, K. (2006). Testing anatomically specified hypotheses in functional imaging using cytoarchitectonic maps. *NeuroImage*, 32(2), 570–582.
- Eickhoff, S. B., Laird, A. R., Fox, P. T., Bzdok, D., & Hensel, L. (2014). Functional segregation of the human dorsomedial prefrontal cortex. *Cerebral Cortex*. <http://dx.doi.org/10.1093/cercor/bhu250>
- Eickhoff, S. B., Paus, T., Caspers, S., Grosbras, M. H., Evans, A. C., Zilles, K., et al. (2007). Assignment of functional activations to probabilistic cytoarchitectonic areas revisited. *NeuroImage*, 36(3), 511–521.
- Eickhoff, S. B., Stephan, K. E., Mohlberg, H., Grefkes, C., Fink, G. R., Amunts, K., et al. (2005). A new SPM toolbox for combining probabilistic cytoarchitectonic maps and functional imaging data. *NeuroImage*, 25(4), 1325–1335.
- Evans, A. C., Janke, A. L., Collins, D. L., & Baillet, S. (2012). Brain templates and atlases. *NeuroImage*, 62(2), 911–922.
- Evans, A. C., Marrett, S., Neelin, P., Collins, L., Worsley, K., Dai, W., et al. (1992). Anatomical mapping of functional activation in stereotactic coordinate space. *NeuroImage*, 1(1), 43–53.
- Farrow, T. F., Zheng, Y., Wilkinson, I. D., Spence, S. A., Deakin, J. F., Tarrier, N., et al. (2001). Investigating the functional anatomy of empathy and forgiveness. *NeuroReport*, 12(11), 2433–2438.
- Frey, S., Kostopoulos, P., & Petrides, M. (2000). Orbitofrontal involvement in the processing of unpleasant auditory information. *European Journal of Neuroscience*, 12(10), 3709–3712.
- Frey, S., & Petrides, M. (2000). Orbitofrontal cortex: a key prefrontal region for encoding information. *Proceedings of the National Academy of Sciences of the United States of America*, 97(15), 8723–8727.
- Goldman-Rakic, P. S. (1984). Modular organization of prefrontal cortex. *Trends in Neurosciences*, 7, 419–429.
- Goldman-Rakic, P. S. (1995). Anatomical and functional circuits in prefrontal cortex of nonhuman primates. In R. S. Jasper H.H., & P. S. Goldman-Rakic (Eds.), *Epilepsy and the functional anatomy of the frontal lobe* (pp. 51–65). New York: Raven Press.
- Goldman-Rakic, P. S., & Schwartz, M. L. (1982). Interdigitation of contralateral and ipsilateral columnar projections to frontal association cortex in primates. *Science*, 216(4547), 755–757.
- Gorno-Tempini, M. L., Pradelli, S., Serafini, M., Pagnoni, G., Baraldi, P., Porro, C., et al. (2001). Explicit and incidental facial expression processing: an fMRI study. *NeuroImage*, 14(2), 465–473.
- Gottfried, J. A., Deichmann, R., Winston, J. S., & Dolan, R. J. (2002). Functional heterogeneity in human olfactory cortex: an event-related functional magnetic resonance imaging study. *Journal of Neuroscience*, 22(24), 10819–10828.
- Gottfried, J. A., O'Doherty, J., & Dolan, R. J. (2002). Appetitive and aversive olfactory learning in humans studied using event-related functional magnetic resonance imaging. *Journal of Neuroscience*, 22(24), 10829–10837.
- Grabenhorst, F., & Rolls, E. T. (2009). Different representations of relative and absolute subjective value in the human brain. *NeuroImage*, 48(1), 258–268.

- Grabenhorst, F., Rolls, E. T., & Bilderbeck, A. (2008). How cognition modulates affective responses to taste and flavor: top-down influences on the orbitofrontal and pregenual cingulate cortices. *Cerebral Cortex*, 18(7), 1549–1559.
- Grabenhorst, F., Rolls, E. T., Margot, C., da Silva, M. A., & Velazco, M. I. (2007). How pleasant and unpleasant stimuli combine in different brain regions: odor mixtures. *Journal of Neuroscience*, 27(49), 13532–13540.
- Grabenhorst, F., Rolls, E. T., Parris, B. A., & d'Souza, A. A. (2010). How the brain represents the reward value of fat in the mouth. *Cerebral Cortex*, 20(5), 1082–1091.
- Gur, R. C., Gunning-Dixon, F., Bilker, W. B., & Gur, R. E. (2002). Sex differences in temporo-limbic and frontal brain volumes of healthy adults. *Cerebral Cortex*, 12(9), 998–1003.
- Hof, P. R., Mufson, E. J., & Morrison, J. H. (1995). Human orbitofrontal cortex: cytoarchitecture and quantitative immunohistochemical parcellation. *Journal of Comparative Neurology*, 359(1), 48–68.
- Iwase, M., Ouchi, Y., Okada, H., Yokoyama, C., Nobezawa, S., Yoshikawa, E., et al. (2002). Neural substrates of human facial expression of pleasant emotion induced by comic films: a PET study. *NeuroImage*, 17(2), 758–768.
- Janata, P., Birk, J. L., Van Horn, J. D., Leman, M., Tillmann, B., & Bharucha, J. J. (2002). The cortical topography of tonal structures underlying Western music. *Science*, 298(5601), 2167–2170.
- Kahnt, T., Chang, L. J., Park, S. Q., Heinze, J., & Haynes, J. D. (2012). Connectivity-based parcellation of the human orbitofrontal cortex. *Journal of Neuroscience*, 32(18), 6240–6250.
- Kringelbach, M. L., O'Doherty, J., Rolls, E. T., & Andrews, C. (2003). Activation of the human orbitofrontal cortex to a liquid food stimulus is correlated with its subjective pleasantness. *Cerebral Cortex*, 13(10), 1064–1071.
- Kringelbach, M. L., & Rolls, E. T. (2004). The functional neuroanatomy of the human orbitofrontal cortex: evidence from neuroimaging and neuropsychology. *Progress in Neurobiology*, 72(5), 341–372.
- Lorenz, J., Minoshima, S., & Casey, K. L. (2003). Keeping pain out of mind: the role of the dorsolateral prefrontal cortex in pain modulation. *Brain*, 126(Pt 5), 1079–1091.
- Luders, E., Toga, A. W., & Thompson, P. M. (2014). Why size matters: differences in brain volume account for apparent sex differences in callosal anatomy: the sexual dimorphism of the corpus callosum. *NeuroImage*, 84, 820–824.
- Mackey, S., & Petrides, M. (2009). Architectonic mapping of the medial region of the human orbitofrontal cortex by density profiles. *Neuroscience*, 159(3), 1089–1107.
- Mackey, S., & Petrides, M. (2010). Quantitative demonstration of comparable arectectonic areas within the ventromedial and lateral orbital frontal cortex in the human and the macaque monkey brains. *European Journal of Neuroscience*, 32, 1940–1950.
- Mahalanobis, P. C., Majumda, D. N., & Rao, C. R. (1949). Anthropometric survey of the united provinces. A statistical study. *Sankhya*, 9, 89–324.
- Maratos, E. J., Dolan, R. J., Morris, J. S., Henson, R. N., & Rugg, M. D. (2001). Neural activity associated with episodic memory for emotional context. *Neuropsychologia*, 39(9), 910–920.
- McNamee, D., Rangel, A., & O'Doherty, J. P. (2013). Category-dependent and category-independent goal-value codes in human ventromedial prefrontal cortex. *Nature Neuroscience*, 16(4), 479–487.
- Merker, B. (1983). Silver staining of cell bodies by means of physical development. *Journal of Neuroscience Methods*, 9(3), 235–241.
- Mesulam, M. M., & Mufson, E. J. (1982). Insula of the old world monkey. III: efferent cortical output and comments on function. *Journal of Comparative Neurology*, 212(1), 38–52.
- Mesulam, M. M., Mufson, E. J., Levey, A. I., & Wainer, B. H. (1983). Cholinergic innervation of cortex by the basal forebrain: cytochemistry and cortical connections of the septal area, diagonal band nuclei, nucleus basalis (substantia innominata), and hypothalamus in the rhesus monkey. *Journal of Comparative Neurology*, 214(2), 170–197.
- Moll, J., de Oliveira-Souza, R., Bramati, I. E., & Grafman, J. (2002). Functional networks in emotional moral and nonmoral social judgments. *NeuroImage*, 16(3 Pt 1), 696–703.
- Morecraft, R. J., Geula, C., & Mesulam, M. M. (1992). Cytoarchitecture and neural afferents of orbitofrontal cortex in the brain of the monkey. *Journal of Comparative Neurology*, 323(3), 341–358.
- Neubert, F.-X., Mars, R. B., Sallet, J., & Rushworth, M. F. S. (2015). Connectivity reveals relationship of brain areas for reward-guided learning and decision making in human and monkey frontal cortex. *Proceedings of the National Academy of Sciences USA*, 112(20), E2695–E2704.
- Ngowyang, G. (1934). Die Cytoarchitektonik des menschlichen Stirnhirns. I. Teil. Cytoarchitektonische Felderung der Regio granularis und Regio dysgranularis. *Monographs of the National Research Institute of Psychology. Academia Sinica*, 7, 1–69.
- O'Doherty, J. P., Dayan, P., Friston, K., Critchley, H., & Dolan, R. J. (2003). Temporal difference models and reward-related learning in the human brain. *Neuron*, 38(2), 329–337.
- O'Doherty, J. P., Deichmann, R., Critchley, H. D., & Dolan, R. J. (2002). Neural responses during anticipation of a primary taste reward. *Neuron*, 33(5), 815–826.
- O'Doherty, J., Kringelbach, M. L., Rolls, E. T., Hornak, J., & Andrews, C. (2001). Abstract reward and punishment representations in the human orbitofrontal cortex. *Nature Neuroscience*, 4(1), 95–102.
- O'Doherty, J., Winston, J., Critchley, H., Perrett, D., Burt, D. M., & Dolan, R. J. (2003). Beauty in a smile: the role of medial orbitofrontal cortex in facial attractiveness. *Neuropsychologia*, 41(2), 147–155.
- Öngür, D., Ferry, A. T., & Price, J. L. (2003). Architectonic subdivision of the human orbital and medial prefrontal cortex. *Journal of Comparative Neurology*, 460(3), 425–449.
- Öngür, D., & Price, J. L. (2000). The organization of networks within the orbital and medial prefrontal cortex of rats, monkeys and humans. *Cerebral Cortex*, 10(3), 206–219.
- Ono, M., Kubik, S., & Abernathey, C. D. (1990). *Atlas of the cerebral sulci*. New York Thieme Medical Publishers, Inc.
- Palomero-Gallagher, N., Mohlberg, H., Zilles, K., & Vogt, B. (2008). Cytology and receptor architecture of human anterior cingulate cortex. *Journal of Comparative Neurology*, 508(6), 906–926.
- Palomero-Gallagher, N., Vogt, B. A., Schleicher, A., Mayberg, H. S., & Zilles, K. (2009). Receptor architecture of human cingulate cortex: evaluation of the four-region neurobiological model. *Human Brain Mapping*, 30(8), 2336–2355.
- Pandya, D. N., Van Hoesen, G. W., & Mesulam, M. M. (1981). Efferent connections of the cingulate gyrus in the rhesus monkey. *Experimental Brain Research*, 42(3–4), 319–330.
- Paxinos, G., Huang, X.-F., & Toga, A. W. (2000). *The rhesus monkey brain in stereotaxic coordinates*. San Diego: Academic Press.
- Perlaki, G., Orsi, G., Plozer, E., Altbacher, A., Darnai, G., Nagy, S. A., et al. (2014). Are there any gender differences in the hippocampus volume after head-size correction? A volumetric and voxel-based morphometric study. *Neuroscience Letters*, 570, 119–123.
- Petrides, M., & Pandya, D. N. (1994). Comparative architectonic analysis of the human and the macaque frontal cortex. In G. J. Boller F. (Ed.), *Handbook of neuropsychology* (Vol. 9, pp. 59–82). Amsterdam (The Netherlands): Elsevier.

- Rao, R. P., & Ballard, D. H. (1999). Predictive coding in the visual cortex: a functional interpretation of some extra-classical receptive-field effects. *Nature Neuroscience*, 2(1), 79–87.
- Rilling, J., Gutman, D., Zeh, T., Pagnoni, G., Berns, G., & Kilts, C. (2002). A neural basis for social cooperation. *Neuron*, 35(2), 395–405.
- Rogers, R. D., Owen, A. M., Middleton, H. C., Williams, E. J., Pickard, J. D., Sahakian, B. J., et al. (1999). Choosing between small, likely rewards and large, unlikely rewards activates inferior and orbital prefrontal cortex. *Journal of Neuroscience*, 19(20), 9029–9038.
- Rolls, E. T. (2000). The orbitofrontal cortex and reward. *Cerebral Cortex*, 10(3), 284–294.
- Rolls, E. T. (2004a). Convergence of sensory systems in the orbitofrontal cortex in primates and brain design for emotion. *The anatomical record. Part A, Discoveries in molecular, cellular, and evolutionary biology*, 281(1), 1212–1225.
- Rolls, E. T. (2004b). The functions of the orbitofrontal cortex. *Brain Cognition*, 55(1), 11–29.
- Rolls, E. T. (2007). The representation of information about faces in the temporal and frontal lobes. *Neuropsychologia*, 45(1), 124–143.
- Rolls, E. T., & Baylis, L. L. (1994). Gustatory, olfactory, and visual convergence within the primate orbitofrontal cortex. *Journal of Neuroscience*, 14(9), 5437–5452.
- Rolls, E. T., Kringelbach, M. L., & de Araujo, I. E. (2003). Different representations of pleasant and unpleasant odours in the human brain. *European Journal of Neuroscience*, 18(3), 695–703.
- Rolls, E. T., O'Doherty, J., Kringelbach, M. L., Francis, S., Bowtell, R., & McGlone, F. (2003). Representations of pleasant and painful touch in the human orbitofrontal and cingulate cortices. *Cerebral Cortex*, 13(3), 308–317.
- Royer, J. P., Hudry, J., Zald, D. H., Godinot, D., Gregoire, M. C., Lavenne, F., et al. (2001). Functional neuroanatomy of different olfactory judgments. *NeuroImage*, 13(3), 506–519.
- Royer, J. P., Zald, D., Versace, R., Costes, N., Lavenne, F., Koenig, O., et al. (2000). Emotional responses to pleasant and unpleasant olfactory, visual, and auditory stimuli: a positron emission tomography study. *Journal of Neuroscience*, 20(20), 7752–7759.
- Sanides, F. (1962). *Die Architektonik des menschlichen Stirnhirns*. Berlin (Germany): Springer.
- Sarkisov, S. A., Filimonoff, I. N., & Preobrazhenskaya, N. S. (1949). *Cytoarchitecture of the human cortex cerebri*. Moscow (Russia): Medgiz.
- Schleicher, A., Amunts, K., Geyer, S., Kowalski, T., Schormann, T., Palomero-Gallagher, N., et al. (2000). A stereological approach to human cortical architecture: identification and delineation of cortical areas. *Journal of Chemical Neuroanatomy*, 20(1), 31–47.
- Schleicher, A., Amunts, K., Geyer, S., Kowalski, T., & Zilles, K. (1998). An observer-independent cytoarchitectonic mapping of the human cortex using a stereological approach. *Acta Stereologica*, 17, 75–82.
- Schleicher, A., Amunts, K., Geyer, S., Morosan, P., & Zilles, K. (1999). Observer-independent method for microstructural parcellation of cerebral cortex: a quantitative approach to cytoarchitectonics. *NeuroImage*, 9(1), 165–177.
- Schleicher, A., Palomero-Gallagher, N., Morosan, P., Eickhoff, S. B., Kowalski, T., de Vos, K., et al. (2005). Quantitative architectural analysis: a new approach to cortical mapping. *Anatomy and Embryology (Berl)*, 210(5–6), 373–386.
- Schleicher, A., & Zilles, K. (1990). A quantitative approach to cytoarchitectonics: analysis of structural inhomogeneities in nervous tissue using an image analyser. *Journal of Microscopy*, 157(Pt 3), 367–381.
- Schnider, A., Treyer, V., & Buck, A. (2000). Selection of currently relevant memories by the human posterior medial orbitofrontal cortex. *Journal of Neuroscience*, 20(15), 5880–5884.
- Seltzer, B., & Pandya, D. N. (1989). Frontal lobe connections of the superior temporal sulcus in the rhesus monkey. *Journal of Comparative Neurology*, 281(1), 97–113.
- Shaw, P., Lalonde, F., Lepage, C., Rabin, C., Eckstrand, K., Sharp, W., et al. (2009). Development of cortical asymmetry in typically developing children and its disruption in attention-deficit/hyperactivity disorder. *Archives of General Psychiatry*, 66(8), 888–896.
- Small, D. M., Jones-Gotman, M., Zatorre, R. J., Petrides, M., & Evans, A. C. (1997). Flavor processing: more than the sum of its parts. *NeuroReport*, 8(18), 3913–3917.
- Small, D. M., Zald, D. H., Jones-Gotman, M., Zatorre, R. J., Pardo, J. V., Frey, S., et al. (1999). Human cortical gustatory areas: a review of functional neuroimaging data. *NeuroReport*, 10(1), 7–14.
- Small, D. M., Zatorre, R. J., Dagher, A., Evans, A. C., & Jones-Gotman, M. (2001). Changes in brain activity related to eating chocolate: from pleasure to aversion. *Brain*, 124(Pt 9), 1720–1733.
- Smith, S. M., Vidaurri, D., Beckmann, C. F., Glasser, M. F., Jenkinson, M., Miller, K. L., et al. (2013). Functional connectomics from resting-state fMRI. *Trends in Cognitive Sciences*, 17(12), 666–682.
- Strasburger, E. (1937). Die myeloarchitektonische Gliederung des Stirnhirns beim Menschen und Schimpansen. I. Teil. Myeloarchitektonische Gliederung des menschlichen Stirnhirns. *Journal für Psychologie und Neurologie*, 47, 461–491.
- Uylings, H. B., Sanz-Arigita, E. J., de Vos, K., Pool, C. W., Evers, P., & Rajkowska, G. (2010). 3-D cytoarchitectonic parcellation of human orbitofrontal cortex correlation with postmortem MRI. *Psychiatry Research*, 183(1), 1–20.
- Vogt, O. (1910). Die myeloarchitektonische Felderung des menschlichen Stirnhirns. *Journal für Psychologie und Neurologie*, 15, 221–232.
- Vogt, B. A., & Pandya, D. N. (1987). Cingulate cortex of the rhesus monkey: II. Cortical afferents. *Journal of Comparative Neurology*, 262(2), 271–289.
- Vogt, C., & Vogt, O. (1919). Allgemeine Ergebnisse unserer Hirnforschung. *Journal für Psychologie und Neurologie*, 25, 279–262.
- Völlm, B. A., de Araujo, I. E., Cowen, P. J., Rolls, E. T., Kringelbach, M. L., Smith, K. A., et al. (2004). Methamphetamine activates reward circuitry in drug naïve human subjects. *Neuropsychopharmacology*, 29(9), 1715–1722.
- Walker, A. E. (1940). A cytoarchitectural study of the prefrontal area of the macaque monkey. *Journal of Comparative Neurology*, 73, 59–86.
- Wicker, B., Perrett, D. I., Baron-Cohen, S., & Decety, J. (2003). Being the target of another's emotion: a PET study. *Neuropsychologia*, 41(2), 139–146.
- Wree, A., Schleicher, A., & Zilles, K. (1982). Estimation of volume fractions in nervous tissue with an image analyzer. *Journal of Neuroscience Methods*, 6(1–2), 29–43.
- Yeterian, E. H., & Pandya, D. N. (1988). Corticothalamic connections of paralimbic regions in the rhesus monkey. *Journal of Comparative Neurology*, 269(1), 130–146.
- Zald, D. H., McHugo, M., Ray, K. L., Glahn, D. C., Eickhoff, S. B., & Laird, A. R. (2014). Meta-analytic connectivity modeling reveals differential functional connectivity of the medial and lateral orbitofrontal cortex. *Cerebral Cortex*, 24(1), 232–248.
- Zatorre, R. J., & Jones-Gotman, M. (1991). Human olfactory discrimination after unilateral frontal or temporal lobectomy. *Brain*, 114(Pt 1A), 71–84.
- Zatorre, R. J., Jones-Gotman, M., Evans, A. C., & Meyer, E. (1992). Functional localization and lateralization of human olfactory cortex. *Nature*, 360(6402), 339–340.

- Zatorre, R. J., Jones-Gotman, M., & Rouby, C. (2000). Neural mechanisms involved in odor pleasantness and intensity judgments. *NeuroReport*, 11(12), 2711–2716.
- Zilles, K., & Amunts, K. (2010). Centenary of Brodmann's map—conception and fate. *Nature Reviews Neuroscience*, 11(2), 139–145.
- Zilles, K., & Amunts, K. (2011). Architecture of the human cerebral cortex: maps, regional and laminar organization. In M. J. Paxinos G (Ed.), *The human nervous system* (3 ed, pp. 836–895). San Diego: Academic Press.
- Zilles, K., Bacha-Trams, M., Palomero-Gallagher, N., Amunts, K., & Friederici, A. D. (2015). Common molecular basis of the sentence comprehension network revealed by neurotransmitter receptor fingerprints. *Cortex*, 63, 79–89.
- Zilles, K., Palomero-Gallagher, N., & Schleicher, A. (2004). Transmitter receptors and functional anatomy of the cerebral cortex. *Journal of Anatomy*, 205(6), 417–432.
- Zilles, K., Schleicher, A., Palomero-Gallagher, N., & Amunts, K. (2002). Quantitative analysis of cyto- and receptor architecture of the human brain. In M. J., & A. W. Toga (Eds.), *Brain Mapping: The Methods* (pp. 573–602). San Diego: Academic Press.